Ancient restoration and production technologies of Roman mortars from monuments placed in hydrogeological risk areas: a case study

Sitzia Fabio[1] · Beltrame Massimo[2] · Columbu Stefano[1] · Lisci Carla[2,3] · Miguel Catarina[2] · Mirão José[2,3]

Abstract

This paper focuses on the study of different Roman mortars (renders, finishing coats), used in the construction and restoration of the *Forum Traiani* thermal baths (Central Sardinia, Italy), a significant example of the Roman-style architecture in Sardinia. The archaeological site is located in a high hydrogeological risk area, due to the cyclical flooding of nearby Tirso river. Moreover, the presence of thermal saline (NaCl-bearing) water spring directly in contact with mortars and building stones, also contributed to structure degradation. An analytical approach, comprising mineralogical-petrographic characterization, physical analysis and particle-size distribution of aggregate, was used for mortars characterization. In addition, pXRD analysis on mortars defined the presence of alteration minerals while the thermal characterization (TGA) gave information about binder hydraulicity degree. Further μ-XRD-associated μ-Raman spectroscopy and μ-FTIR were utilized for pigments identification on frescos. Interesting results came from two wall stratigraphic series of mortars, highlighting construction stages, ancient restoring interventions and waterproofing methods. The main pigments used on red, yellow and black frescoes were red ochre, goethite and wood charcoal respectively.

Keywords Ancient restoration · Roman mortars · Paintings · Hydrogeological risk

Introduction

The scientific contributions on the ancient mortars and geo-materials are very useful to deepen the knowledge about the production technologies, working techniques and provenance of raw materials in Roman age (Antonelli et al. 2014; Cardoso et al. 2014; Columbu et al. 2017, 2018b, 2018d, 2018e, 2019a, 2019b; Columbu 2017, 2018; Columbu and Garau 2017; Lezzerini et al. 2016, 2018; Miriello et al. 2015, 2019; Raneri et al. 2018; Ramacciotti et al. 2019; Secco et al. 2018; Secco et al. 2019; Jackson et al. 2013; Piovesan et al. 2013; Verdiani and Columbu 2010).

The archaeological site of *Forum Traiani* or *Aquae Ypsitanae* (Fig. 1) is a late Republican settlement built by Trajan Emperor as a market centre between the inland communities and Romans settlements located by the Oristano gulf (central-west Sardinia). The archaeological area is located in Fordongianus municipality, Sardinia, Italy (39° 59′ 48.71″ N–8° 48′ 30.29″ E, Fig. 1).

According to the latest archaeological works (Zucca 1986; Meloni 1990), the urban settlement is in the form of a quadrangle with an expansion of 4 ha (Serra and Bacco 1998).

The site comprises a thermal plant chronologically divided into two sub-systems—*Terme I* and *Terme II*, (Fig. 2). *Terme I* is considered the original nucleus referred to I Cent. AD (Serra and Bacco 2014). In *Terme I* sub-system, a spring of NaCl-bearing waters (local name: *Caddas*, coming out water temperature: 54 °C) is still present.

Forum Traiani is one of the three hydrotherapy baths of ancient Sardinia apart from *Aquae Lesitanae* (Benetutti) and the *Aquae Neapolitanae* (Sardara).

✉ Sitzia Fabio
fasitzia@tiscali.it

1   Department of Chemical and Geological Sciences, University of Cagliari, Cittadella Universitaria di Monserrato (Blocco A), 09042 Monserrato, Cagliari, Italy

2   HERCULES Laboratory, Institute for Advanced Studies and Research, University of Évora, Largo Marquês de Marialva 8, 7000-809 Evora, Portugal

3   Geosciences Department, School of Sciences and Technology, University of Évora, Rua Romão Ramalho 59, 7000-671 Evora, Portugal

🍁 Springer

Fig. 1 *Forum Traiani* thermal baths system: **a** localization of the archaeological site, **b** external *natatio,* southern view (Terme I), **c** external *natatio*, South-West view (Terme I), **d** external *natatio*, South-East view (Terme I), **e** main *frigidarium* room in Terme II, **f** ruins of column in East courtyard (Terme II), **g** Barrel vault ruins of Terme I *natatio*. Photos by Fabio Sitzia
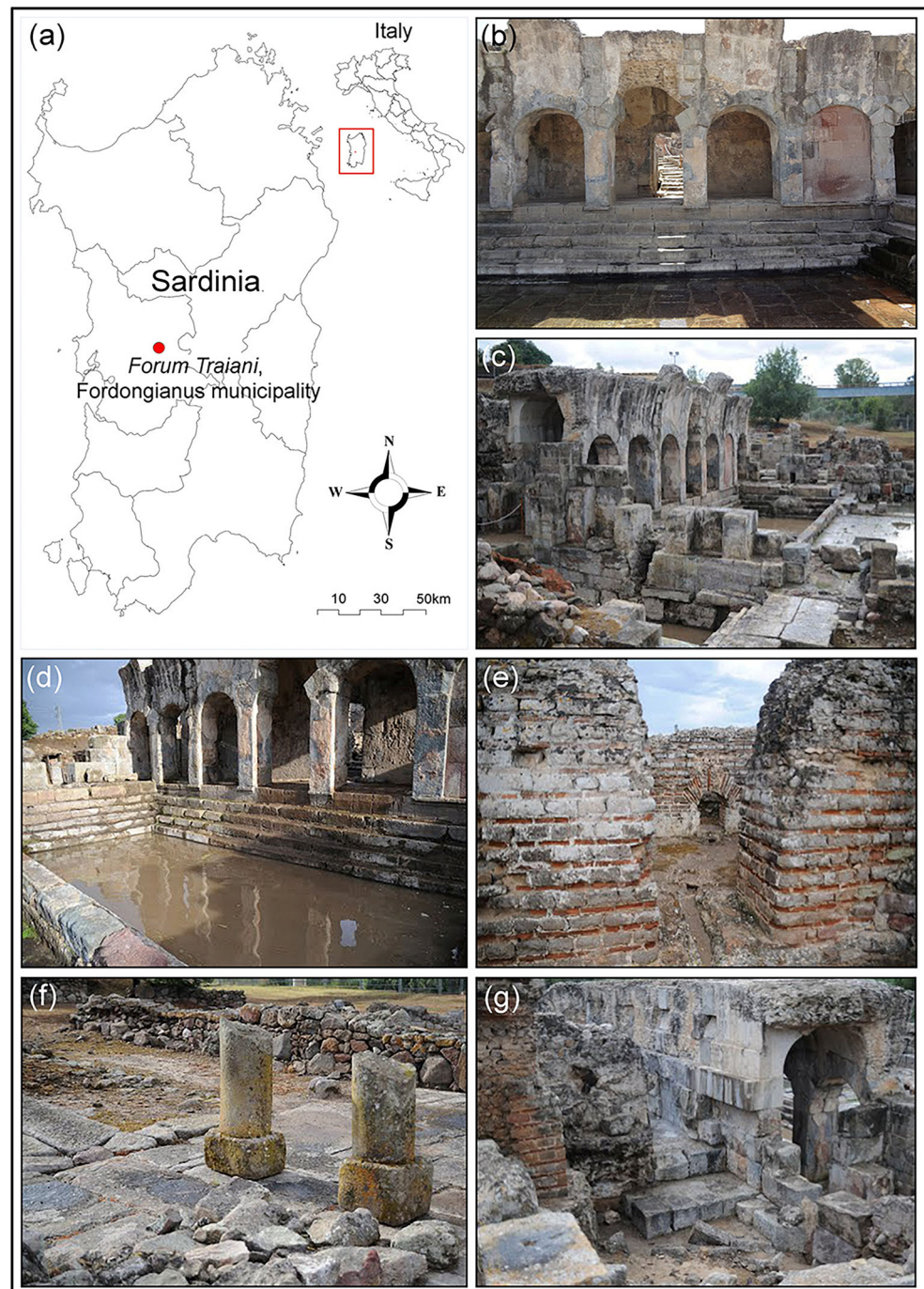
The second core, Terme II, is from II-IV Cent. AD (Serra and Bacco 2014; Angiolillo 1998).

Forum Traiani has not so far been affected by systematic archaeological surveys. The archaeological knowledge is composed by a collection of data from different historical phases of Roman and post-Roman times. The site was partly brought to light in the first excavation campaign during 1990s (Mastino 2005; Zucca 2004).

Recent studies about *Forum Traiani* focused on 3D graphic processing of *Ninfeo* and *Natatio* (Serra and Bacco 2014) and

on the mosaic of Flavius Rogatianus (Quattrocchi 2018). Some authors analysed the materials used for construction by using physical-chemical and optical microscopy (OM) characterization, thereby defining the mining techniques and their specific use over the centuries (Argiolas 2006; Sitzia 2019). Up to now, no documentation has been found on the characterization of the mortars belonging to the site.

The monument is developed on fluvial terraces located on the left bank of Tirso river, the longest river of Sardinia. Basing on hydrogeological evidence (PAI, Piano di assetto
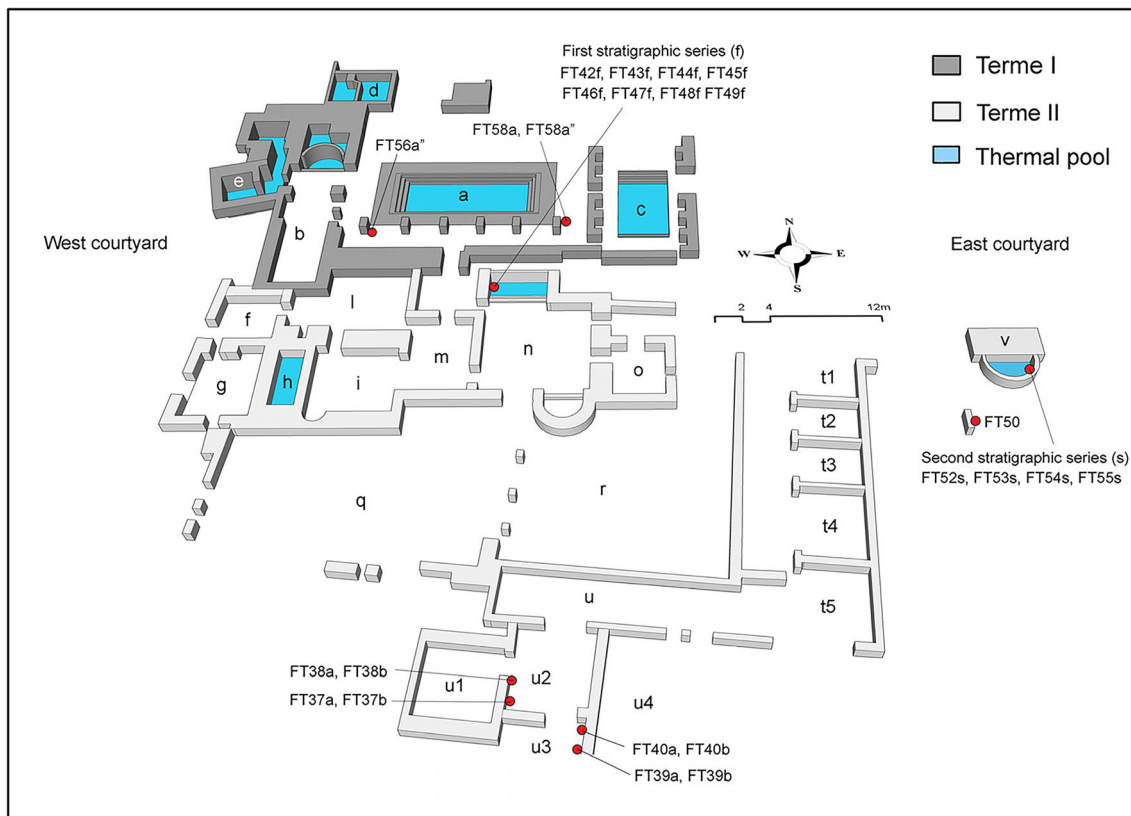
Fig. 2 *Forum Traiani* archaeological site with sampling points in red: a = *natatio*; b = *apodyterium*; c = *ninfeo*; d = thermal pool; e = uptake pool; f, g = furnaces; h = *calidarium pool*; i, l = *calidarium*; m = *tepidarium*; n = *frigidarium*; o = *apodyterium*; q = courtyard access; r = gym; t1, t2, t3, t4, t5 = *tabernae*; u, u1, u2, u3, u4 = housing structures; v = water tank. 3D graphic processing by Fabio Sitzia

idrogeologico regione Sardegna, year 2006), the Tirso river overflows every 50 years on average, it is reasonable to think that during Roman times, the thermal area was flooded several times. Assuming that only some of these natural events may have truly damaged the structures of the thermal bath, we suppose that at least some of them forced Roman maintainers to intervene in order to restore the structures.

Despite the advanced degradation of structures and materials of *Forum Traiani*, inside *Terme II Frigidarium* (Fig. 2) and in the East courtyard, there are some important evidences about two thick plaster stratigraphies, still adhering to the original structures. Given their importance, they have been sampled and in-detail studied to firstly define their composition and secondly to understand the constructive meaning-production, application and restoration technologies.

According to this last interesting archaeological evidence about the stratigraphies, some hypotheses about the use of the thermal plant in Roman times were made by multi-analytical and multi-disciplinary approaches. In particular, we try to understand if (i) the site may have been temporarily abandoned, due to important geological events (i.e. flooding) which caused damage to the structures and construction materials requiring new laying of plasters, (ii) rooms could have had a different intended use during the time, (iii) considering that in

the *Frigidarium* (where the first stratigraphy was collected) it had a bathtub, the plaster cycle interventions could be require for solving the problems due to the wall humidity rising or the presence of saline thermal waters used in the room.

This research aims to understand ancient Roman production and restoration technology in construction of a thermal bath located in a high hydrogeological risk area. This particularity makes *Forum Traiani* an interesting case study.

In order to study the aforementioned aims, particle-size, geochemical, thermal-gravimetric analysis (TGA), mineralogical (pXRD), physical and mechanical analyses were performed in order to understand mortars characteristics.

The main for studying the frescoes is to define the typology and binder characteristics of original Roman paintings with the help of μ-XRD, μ-Raman and μ-FTIR.

Materials and methods

Materials

The wall plaster applied to the building generally consists of three mortar layers. From internal to external, the first is a ceramic fragment render (*Trullissatio*), follow by a lime

render and a finishing coat. These three layers were followed by a marble slabs or frescoes.

A total of 24 samples of mortars, of which, 8 *Trullissatio*, 8 lime renders and 8 finishing coats, were collected according to Table 1 and Figs. 2 and 3. Paintings are present on the surface of all finishing coats except the sample FT55s (Table 1).

Sampling was realized in agreement with local authorities, according to CNR-ICR (1990) Nor.Ma.L. 3/80 standard.

The samples (Fig. 3) are appointed with the acronym FT (*Forum Traiani*). A first wide stratigraphic series of mortars (called *f*) was collected in the *Frigidarium* (room "n", Fig. 2) and it consists three layers of lime render-finishing coat and two *Trullissatio layers* (FT42f, 43f, 44f, 45f, 46f, 47f, 48f, 49f).

A second stratigraphic series of mortars (called *s*) was collected on a water tank (structure v, Fig. 2) and it consists of two *Trullissatio* layers, a lime render and a finishing coat (FT52s, 53s, 54s, 55s).

Minor stratigraphic series are only represented by two samples of lime render—finishing coat (e.g. FT37a–FT37b, FT38a–FT38b, FT39a–FT39b, FT40a–FT40b). Other samples, individually collected, as FT50, FT56a′, FT56a″ and FT58a′ are represented by *Trullissatio*.

Methods

Petrographic determinations (OM) were carried out by optical polarized microscope Leitz Wetzlar on 30 μm thin sections. Modal analysis of aggregates has been determined with points counter on about 300 points for each thin section. Circularity of aggregates was estimated by synoptic table according to Krumbein (1941).

For pXRD and μ-XRD analyses, a Bruker AXS D8 Discovery XRD with a CuK$_\alpha$ source, operating at 40 kV and 40 mA, and a Lynxeye 1-dimensional detector was used. Scans were performed from 3 to 75°2θ, with 0.05°2θ step and 1 s/step measuring time by point. Diffract-Eva software from Bruker with PDF-2 mineralogical database (International Centre for Diffraction Data—ICDD) was utilized to interpret the scans. During the μ-XRD experiments, a Goebel mirror and 1-mm collimator were employed.

Raman microscopy and μ-FTIR spectroscopy were used to identify the chromophore phases present in the painted.

μ-FTIR was used to detect the presence of a pigment binder utilized during the application of the painted layers. To perform the analyses, a small amount of

Table 1 Sampling Log according to Nor.Ma.L 3/80 normative. Sampling elevation was measured with respect to the floor level

Mortar	Sampling point	Function	Sampling elevation (cm)	Decay, alteration forms or depositions
FT48f	*Frigidarium*	Ceramic fragments render (*Trullissatio*)	163	None
FT49f	*Frigidarium*		163	None
FT50	Wall ruin (East courtyard)		70	Biological patina
FT52s	Water tank (East courtyard)		− 40	None
FT53s	Water tank (East courtyard)		− 40	None
FT56a″	*Natatio*		70	None
FT58a′	*Natatio*		162	None
FT58a″	*Natatio*		162	None
FT37a	Housing structure 2	Lime render	56	None
FT38a	Housing structure 2		55	None
FT39a	Housing structure 3		49	None
FT40a	Housing structure 3		53	None
FT42f	*Frigidarium*		60	None
FT44f	*Frigidarium*		60	None
FT46f	*Frigidarium*		163	None
FT54s	Water tank (East courtyard)		− 40	None
FT37b	Housing structure 2	Finishing coat	56	Painting traces
FT38b	Housing structure 2		55	Painting traces
FT39b	Housing structure 3		49	Painting traces
FT40b	Housing structure 3		53	Painting traces
FT43f	*Frigidarium*		60	Painting traces
FT45f	*Frigidarium*		163	Painting traces
FT47f	*Frigidarium*		163	Painting traces
FT55s	Water tank (East courtyard)		− 40	None

Fig. 3 Mortars of *Forum Traiani*: **a** fragment of rubble brick render *Trullissatio* FT50, **b** stratigraphic series lime render-finishing coat FT37a-FT37b. Paintings are present on external surface of FT37b, **c** stratigraphic series lime render-finishing coat FT38a-FT38b, **d** part of wide first "f" stratigraphic series with samples FT45f, FT46f, and FT47f, **e** red paintings on sample FT40b, **f** red and black paintings on finishing coat FT43f
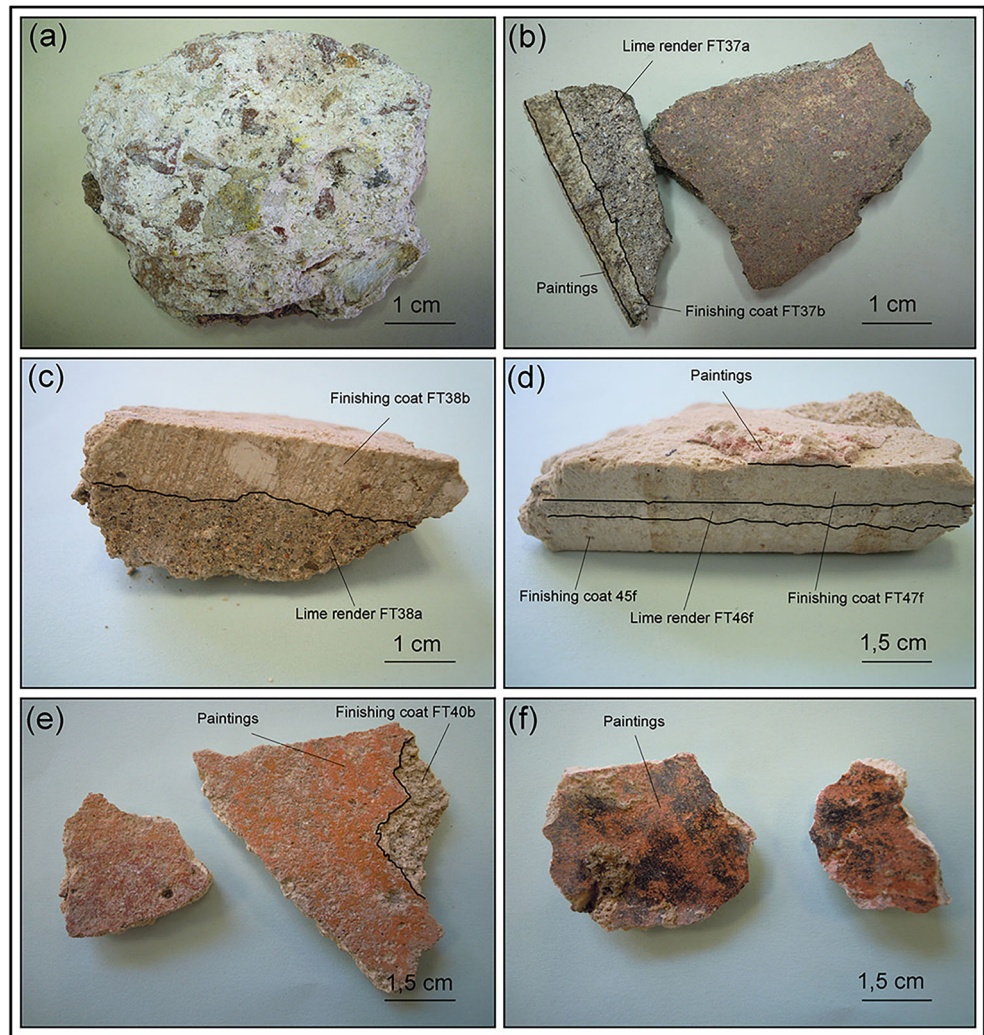
sample (diameter of about 200 μm) was mechanically removed using a small razor blade. μ-Raman analyses were performed using a HORIBA XPlora spectrometer equipped with a diode laser of 28 mW operating at 785 nm, coupled to an Olympus microscope. Raman spectra were acquired in extended mode in the 100–1400 cm^{-1} region. The equipment was previously calibrated using a silicon reference sample. The laser was focused with an Olympus × 50 lens, 10% of the laser power on the sample surface (5 s of exposure, 5 cycles of accumulation). Results were acquired and interpreted using LabSPEC5 software. μ-FTIR spectroscopy was performed in the mid-infrared region (4000–650 cm^{-1}) using a Brüker Hyperion 3000 Tensor 27 equipped with a single point MCT detector cooled with liquid nitrogen. The results were acquired in transmission mode, using a S.T. Japan diamond anvil compression cell. Spectra were collected using OPUS 7.2 software with spectral resolution of 4 cm^{-1} and 32 scans. For the Raman microscopy results, a comparison with reference bibliography and exploring RRUFF database (http://rruff.info/, Lafuente et al. 2016) was performed.

Physical tests were performed on cubic specimens ($15 \times 15 \times 15 \pm 5$ mm) dried at 105 ± 5 °C to determine dry masses (m_D) by analytical balance Sartorius R9. The real and the solid volumes (V_R and V_S respectively) were determined by helium pycnometer UP1000 Quantachrome. The wet mass (m_W) of the samples was determined after 10 days of immersion. The bulk volume V_B was calculated as:

$$V_B = ((m_W - m_{HY})/\rho_{W25°C})100$$

where m_{HY} is the hydrostatic mass of the wet specimen and $\rho_{W25°C}$ is the water density (0.9970 g/cm^3) at temperature of 25 °C. Water and helium open porosities (ΦH_2O, ΦHe), helium closed porosity (Φ_C) were calculated as:

$$\Phi H_2O\ (\%) = [(m_W - m_D)/\rho_{WT25°C}]/V_B)100$$

$$\Phi He \ (\%) = ((V_B - V_R)/V_B))100$$

$$\Phi_C \ (\%) = ((V_R - V_S)/\ V_S))100$$

Total porosity was calculated as:

$$\Phi_T \ (\%) = \Phi He + \Phi_C$$

Bulk, real and solid densities (ρ_B, ρ_R, ρ_S, g/cm^3), were computed as:

$$\rho_B = m_D/V_B$$
$$\rho_R = m_D/V_R$$
$$\rho_S = m_D/V_S$$

Weight imbibition coefficient (CI_W) and saturation index (S.I.) were computed as:

$$CI_W(\%) = ((m_w - m_D)/m_D)100$$
$$S.I.(\%) = (\Phi H_2O/\Phi He)100$$

Point load index (Is_{50}) was determined with Point Load Tester (mod. Controls D550 Instrument). The compressive strength (R_C) and the tensile strength (R_T) were indirectly calculated according to ISRM normative (Franklin 1985) and Palmstrom (Palmström 1995).

The binder/aggregate ratio of the mortars was determined by acid dissolution of binder fraction (with HCl 13% concentrated solution) for 48-h immersion according to the method of Columbu et al. (2015, 2016, 2018a, 2018c).

The particle-size distribution (PSD) of residual aggregate was obtained using sieves with mesh openings of 8000, 4000, 2000, 1000, 500, 250, 125 and 63 μm.

Thermo-gravimetric analysis on the binder (TGA) was carried out using a balance Netzsch STA449F3jupiter. The measurements were performed under Ar flow (60 mL/min). Samples were placed in platinum crucibles and scanned in the temperature range from 30 to 850 °C with heating rate of 10 °C/min. Before TGA analysis binder was manually separate to the aggregate by stereo-microscope Wild Heerbrugg.

Results

Macroscopic observation and mineralogy characterization (OM)

By macroscopic observations, the binders of mortars show a colour surface variable from grey (CIELAB 70*-1*6) to white (CIELAB 90*-4*2) (Fig. 3a–d). In finishing coats, the binders always present a light-white base colour CIELAB 73*-4*0 with traces of red (CIELAB 60*32*9), orange (CIELAB 55*8*26) and black paintings (CIELAB 13*5*-2), (Fig. 3b–f).

The binder has a medium degree of cohesion with sub-circular lime-lumps up to 2–6% vol. and 1 mm up to 1-cm dimension. Sometimes binders are affected by fractures with average ≈ 10 μm opening and ≈ 750 μm spacing.

As shown in Table 2, the aggregate is represented by rock fragments, ceramic fragments, bioclasts, felsic crystal-clasts (i.e. quartz, plagioclase, K-feldspar, muscovite), mafic crystal-clasts (i.e. opaque minerals) and rare charcoal.

In *Trullissatio*, rock rubble aggregate is detected in percentages from 0.8 to 35.8 with an average of 14.5 ± 14.4%. Rock aggregates present circularity (C) between 6 and 7 with dimensions from 0.2 to 1 cm. This aggregate is mainly represented by local rhyolite and rhyodacite, subordinately of granitoids, lidites and very rare marble (Fig. 4e). Ceramic fragment aggregates (on average 73.7 ± 15.5%, Table 2) show low values of circularity (C < 0.3) and dimensions from 0.2 to 2.5 cm. These present two different compositions: calcareous paste (≈ 80%) and siliceous paste (≈ 20%). Ceramic fragments show different percentage from 1 to ≈ 23% and different particle-size distribution of temper (Fig. 4a–d). This is sometime randomly oriented (Fig. 4a–d), but other times, it presents weak alignment (Fig. 4c). A percentage of 11.7 ± 5.9 of the aggregates in *Trullissatio* mortars is represented by felsic crystal-clasts belonging to the sands with following composition: 6/10 of quartz, 3/10 of plagioclase-K-feldspar and 1/10 of muscovite. Rare mafic crystal-clasts in percentages of 0.1% are attributed to opaques. Crystal-clasts present well-rounded shape (6 < C < 7) and dimensions from 0.1 to 1.5 mm.

In sample FT53s, collected from the internal plaster of water tank, a total of 0.1% of residual charcoal have been identified and characterized by species. A fragment of 500-μm diameter shows the presence of pluriseriate and uniseriate rays in tangential cross-section typical of oak wood (*Quencus* sp.), autochthonous species still present in *Fordongianus-Traiani* countryside. It is not clear if charcoal was accidentally produced during lime firing or represents a mineral addition. In this regard, the waterproofing properties of charcoal dust in mortars were already known by Vitruvius (Wetmore and Vitruvius Morgan 2010; Cagnana 2000). These recommendations, handed down in the Middle Ages, were taken up by Cennini (1859), and Oliver et al. (2006) who recommended the use of oak charcoal dust to create a waterproofing layer.

In the lime renders, rock aggregates are detected in percentages from 49.5 to 71.2% (Table 2) with an average of 60.5 ± 6.4%. These aggregates have the same circularity of *Trullissatio* mortars (i.e. 6 < C < 7) but with lower dimensions from 0.2 to 1 cm. Rock rubble mainly consists in local rhyolite and rhyodacite, granitoids and lidites. Ceramic fragment aggregates are absent and bioclasts are present in 0.1% in sample FT38a. A percentage of 39.4 ± 6.5% of the aggregates (Table 2) are felsic crystal-clasts belonging to sands with composition of 6/10 quartz, 3/10 plagioclase-K-feldspar and 1/

Table 2 Modal percentage analysis of mortar aggregates (italic differentiates standard deviations and arithmetic averages from the rest of the data)

Mortar	Function	Rock rubble (%)	Ceramic fragments (%)	Bioclasts (%)	Felsic crystal-clasts (%)	Mafic crystal-clasts (%)	Charcoal (%)
FT48f	Ceramic fragments render (*Trullissatio*)	30	50.2	0	19.8	0	0
FT49f		29.1	59.6	0	11.1	0.2	0
FT50		0.8	94.4	0	4.7	0.1	0
FT52s		8.2	85.8	0	6	0	0
FT53s		35.8	58.9	0	5.1	0.1	0.1
FT56a′		5.3	81.9	0	12.7	0.1	0
FT58a′		2.7	80.6	0	16.6	0.1	0
FT58a″		4.4	78.3	0	17.3	0	0
Arithmetic average		*14.5*	*73.7*	*0*	*11.7*	*0.08*	*0.01*
Standard deviation		*14.4*	*15.5*	*0*	*5.9*	*0.07*	*0.04*
FT37a	Lime render	49.5	0	0	50.5	0	0.1
FT38a		59.8	0	0.1	40.1	0	0.1
FT39a		59.8	0	0	40.2	0	0.1
FT40a		63.7	0	0	36.2	0.1	0.1
FT42f		71.2	0	0	28.5	0.2	0.1
FT44f		57.3	0	0	42.7	0	0
FT46f		57.4	0	0	42.5	0.1	0
FT54s		65.1	0	0	34.5	0.2	0.2
Arithmetic average		*60.5*	*0*	*0.01*	*39.4*	*0.08*	*0.09*
Standard deviation		*6.4*	*0*	*0.04*	*6.5*	*0.09*	*0.06*
FT37b	Finishing coat	2.1	0	0.1	97.7	0.1	0
FT38b		2.4	0	0	97.5	0.1	0
FT39b		4.8	0	0	95	0.2	0
FT40b		4.5	0	0	95.4	0.1	0
FT43f		8.8	0	0	91.2	0	0
FT45f		7.5	0	0	92.5	0	0
FT47f		30	0	0	70	0	0
FT55s		0	0	0	100	0	0
Arithmetic average		*7.5*	*0*	*0.01*	*92.4*	*0.06*	*0*
Standard deviation		*9.5*	*0*	*0.04*	*9.5*	*0.07*	*0*

10 muscovite (Fig. 4f). Mafic minerals consist of opaques (0.1%). Only the samples FT42f and FT54s contain charcoal in percentages of 0.1 and 0.2%, respectively. In lime renders, crystal-clasts have been identified with percentages from 28.5 to 50.5% with well-rounded shape ($6 < C < 7$) and dimensions from 0.1 to 1.5 mm. Charcoal (Fig. 4g) is present in almost all the sample.

In finishing coat, rock rubble is detected in percentages from 0 to 30% with average of $7.5 \pm 9.5\%$. These have the same circularity of other mortars ($6 < C < 7$) and intermediate dimensions from 0.2 to 1.5 cm. Large amount of aggregates consists of felsic sands ($92.4 \pm 9.5\%$) with prevailing quartz, K-feldspar, plagioclase. Mafic crystal-clasts are represented by opaque.

Bioclasts are only present in the sample FT37b (0.1%), including bivalves (Fig. 4h), echinoderms and coralline algae.

Particle-size distribution and binder/aggregate ratio

Binder/aggregate ratio data of the different mortar groups are reported in Table 3. According to Vitruvius (Pollione n.d. 15 BC), mortars should present a volume of aggregate correlated with the cast thickness (T).

In the case of *Trullissatio*, the low binder/aggregate ratio ($0.20 < B/A < 1.75$ with average 0.51) is associated with a great cast thickness (i.e. $0.8 < T < 5$ cm). In lime render, binder/aggregate ratio is more homogeneous ($0.48 < B/A < 0.78$ with average 0.68) with a lower cast thickness ($0.4 < T < 1.5$ cm).

Fig. 4 Mortars of *Forum Traiani* in thin section (NX photos): **a** fragment of ceramic with ≈1% vol. of temper (*Trullissatio* FT58a″), **b** fragment of ceramic with ≈ 14% vol. of temper, various PSD (sample FT56a′), **c** fragment of ceramic with ≈ 15% vol. of temper, uniform PSD (sample FT56a′), **d** fragment of ceramic with ≈ 23% vol. of temper, very various PSD, **e** marble fragment (FT49f), **f** Crystal clasts of quartz, plagioclase and muscovite (FT39a), **g** charcoal fragment in the sample FT37a, **h** bioclast of bivalve in finishing coat FT37b. Photos by Fabio Sitzia
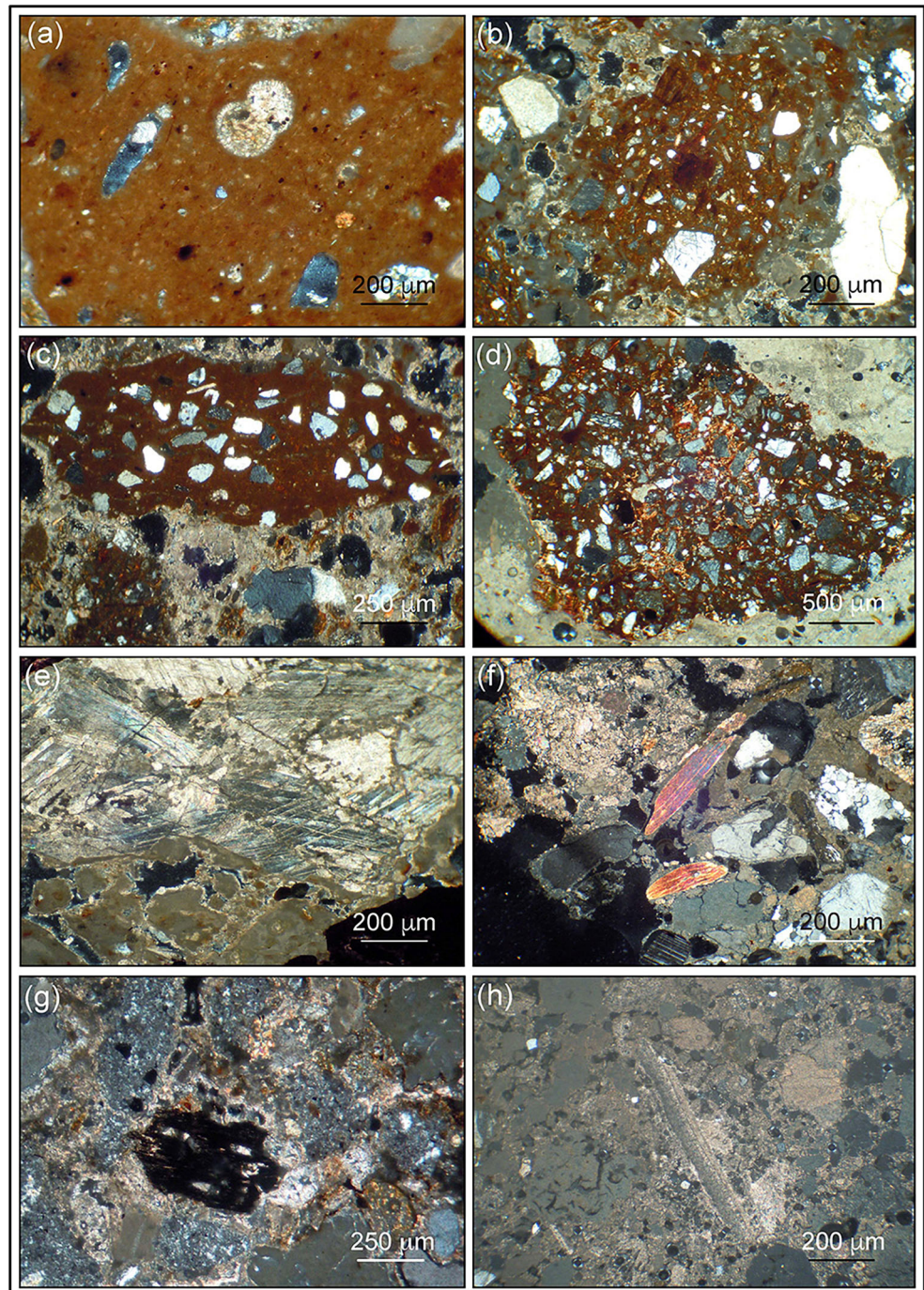
The highest values of binder-aggregate ratio are recorded in the finishing coats ($2.02 < B/A < 18.92$ with average 5.38) with the lowest cast thickness ($T \approx 0.4$ mm).

As regards the particle-size curves (Tables 3, 4 and 5), *Trullissatio* samples (FT48f, FT49f, Fig. 5a, b) and FT52s, FT58a″ are characterized by higher hold masses (d_H) on 4000 and secondly 2000-μm sieves, highlighting an aggregate mainly constituted by granules according to Wentworth

(1922) classification. Samples FT50 (Fig. 5c, d) and FT58a′ are different, showing $d_H = 1000$–2000 μm and 2000–1000 μm, highlighting an aggregate mainly constituted by very coarse sand (Table 3). Small grain size gaps are shown in FT53s and FT56a′ samples pointing out a bimodal PSD due to the presence of ceramic fragments aggregate and monomineralic clasts with different particle sizes. In the first, there is a slight grain size gap on 1000 μm (12.9%) compared with the nearby sieves of 2000 μm (23.9%) and 500 μm

Table 3 Particle-size distribution (PSD) of mortar aggregates: hold mass percentage according to UNI 3121 sieve series, B/A, binder/aggregate ratio

Mortar	Function	B/A	Hold mass percentage								
			8000 μm	4000 μm	2000 μm	1000 μm	500 μm	250 μm	125 μm	63 μm	< 63 μm
FT48f	Ceramic fragments render	1.75	15.61	35.32	18.89	6.65	9.45	6.45	3.53	1.64	2.46
FT49f	(*Trullissatio*)	0.46	15.76	38.63	18.6	8.89	7.88	4.82	2,51	2.38	0.53
FT50		0.23	0	0	26.13	28.34	19.1	9.75	6.63	4.02	6.03
FT52s		0.23	0	26.43	27.13	15.37	11.48	8.94	5.08	3.48	2.09
FT53s		0.66	0	0	23.90	12.91	19.92	17.29	11.63	6.37	7.98
FT56a′		0.2	4.64	32.48	12.06	13.09	16.24	11	4.92	2.78	2.79
FT58a′		0.31	0	5.61	31.78	24.3	18.69	8.41	5.61	3.74	1.86
FT58a″		0.2	5.77	32.54	21.52	12.07	11.02	6.29	5.54	2.62	2.63
FT37a	Lime render	0.71	0	0	7.61	11.19	43.63	32.71	2.52	0.59	1.75
FT38a		0.73	0	0	7.76	11.44	38.55	35.11	4.29	1.03	1.82
FT39a		0.63	0	19.82	9.35	11.06	25.58	28.52	3.47	1.1	1.1
FT40a		0.76	0	23.74	11.43	6.24	25.05	24.48	4.66	1.76	2.64
FT42f		0.72	0	14.96	7.84	10.01	29.39	32.36	3.31	1.07	1.06
FT44f		0.6	0	0.95	15.24	24.76	20.95	16.19	16.19	3.81	1.91
FT46f		0.78	0	0	9.05	8.99	24.71	49.33	4.94	1.19	1.79
FT54s		0.48	0	22.36	14.91	14.16	14.49	14.78	8.53	5.8	4.97
FT37b	Finishing coat	4.16	0	0	31.79	34.7	17.22	7.55	6.09	2.65	0
FT38b		5.16	0	0	28.28	36.55	15.17	9.66	6.21	3.45	0.68
FT39b		2.02	0	18.56	9.28	11.34	22.68	29.9	5.15	2.06	1.03
FT40b		2.3	0	13.56	13.25	12.13	21.3	27.52	6.12	4.08	2.04
FT43f		4.39	0	0	0	9.79	10.27	67.49	3.99	6.04	2.42
FT45f		3.18	0	0	26.79	33.93	20.54	16.07	2.67	0	0
FT47f		2.94	0	0	24.71	31.03	23.18	15.9	5.18	0	0
FT55s		18.92	0	0	0	0	19.42	16.5	64.08	0	0

(19.9%, Table 3). In sample FT56a′ (Fig. 5e, f), there is a slight grain size gap on 2000 μm (12.1%) and 1000 μm (13.1%) compared with immediately nearby sieves of 4000 μm (32.5%) and 500 μm (16.2%). As can be seen from Table 5, in the analysis of midpoint passing diameters $D_{10\%}$ and $D_{60\%}$, all the *Trullissatio* mortars show various particle-size with uniformity coefficient $8.26 < U < 16$.

As regards lime render, the samples FT37a (Fig. 6a, b), FT38a and FT46f (Table 3) show hold masses percentages centred to sieves of 500 and 250 μm with aggregate classifiable as medium sand. Interesting it is the case of the samples FT39a, FT40a and FT42f, where $d_{\mathrm{H}} = 500$–250 μm, with a strong percentage of hold mass in the sieves of 4000 μm pointing out a bimodal particle-size distribution. In the case of FT54s (Table 4, Fig. 6c, d), the aggregate is distributed in similar percentages in the sieves of 2000, 1000, 500 and 250 μm determining a various particle-size distribution with $U = 15$ (Table 5). FT54s and FT44f are the only mortar with various PSD in the group of lime renders while the other samples present uniform aggregate with $1.89 < U < 4.07$.

In finishing coat, (Table 3) hold masses aggregate percentages differ from sample to sample showing a high particle-size inhomogeneity. In FT37b, FT38b (Fig. 6e, f), FT45f and FT47f sample holding is prevalent on sieves of 1000 and 2000 μm (very coarse sand). FT39b and FT40b samples show $d_{\mathrm{H}} = 250$–500-μm sieves, highlighting a medium sand aggregate. In FT43f sample, hold mass is very high on 250-μm sieve (67.5%), showing uniform particle sizes with $U = 1.6$. Uniform particle-size is identified all the samples except to FT37b and FT38b, where $U = 5.7$ and 6.4 respectively (Table 5). According to these results, the trend B/A–cast thickness (T) indicated by Vitruvius seems to be respected in all the groups. However, the aggregate PSD in most of the lime renders samples and finishing coats are uniform, contrary to what was suggested by the Roman architect.

Physical-mechanical properties

Physical-mechanical characteristic of mortars are reported in Tables 6 and 7 and in Fig. 7.

Table 4 Particle-size distribution (PSD) of mortar aggregates: cumulative passing percentage according to UNI 3121 sieve series

Mortar	Function	Cumulative passing percentage								
		8000 μm	4000 μm	2000 μm	1000 μm	500 μm	250 μm	125 μm	63 μm	< 63 μm
FT48f	Ceramic fragments render (*Trullissatio*)	84.39	49.07	30.18	23.53	14.08	7.63	4.10	2.46	0
FT49f		84.24	45.61	27.01	18.12	10.24	5.42	2.91	0.53	0
FT50		100	100	73.87	45.53	26.43	16.68	10.05	6.03	0
FT52s		100	73.57	46.43	31.06	19.58	10.64	5.57	2.09	0
FT53s		100	100	76.1	63.19	43.27	25.98	14.35	7.98	0
FT56a′		95.36	62.88	50.81	37.73	21.49	10.49	5.57	2.79	0
FT58a′		100	94.39	62.61	38.31	19.63	11.21	5.61	1.86	0
FT58a″		94.23	61.69	40.17	28.10	17.08	10.79	5.25	2.63	0
FT37a	Lime render	100	100	92.39	81.2	37.57	4.86	2.34	1.76	0
FT38a		100	100	92.24	80.8	42.25	7.14	2.85	1.81	0
FT39a		100	80.18	70.83	59.78	34.19	5.67	2.2	1.1	0
FT40a		100	76.26	64.84	58.59	33.54	9.06	4.4	2.64	0
FT42f		100	85.04	77.2	67.19	37.80	5.44	2.13	1.06	0
FT44f		100	99.05	83.81	59.05	38.1	21.91	5.72	1.91	0
FT46f		100	100	90.95	81.96	57.25	7.92	2.98	1.79	0
FT54s		100	77.64	62.73	48.57	34.08	19.3	10.77	4.97	0
FT37b	Finishing coat	100	100	68.21	33.51	16.29	8.74	2.65	0	0
FT38b		100	100	71.72	35.17	20	10.34	4.14	0.68	0
FT39b		100	81.44	72.16	60.82	38.14	8.25	3.09	1.03	0
FT40b		100	86.44	73.19	61.06	39.76	12.23	6.12	2.04	0
FT43f		100	100	100	90.21	79.94	12.45	8.46	2.42	0
FT45f		100	100	73.21	39.29	18.75	2.68	0	0	0
FT47f		100	100	75,29	44,25	21,07	5,17	0	0	0
FT55s		100	100	100	100	80,58	64,08	0	0	0

In Fig. 7a, histogram shows the values of average solid, real and bulk density with standard deviations of the mortar groups.

In *Trullissatio*, the solid density is less (2.56 ± 0.07 g/cm^3), because this property is mainly affected by the high amount of ceramic fragments ($73.7 \pm 15.5\%$, Table 2). In fact, ceramic fragments with solid density of 2.5 g/cm^3 contribute to lightening of the cast.

In lime render, the average solid density is higher (2.69 ± 0.03 g/cm^3, Table 6) due to the absence of ceramic fragments (generally with low density, about 2.5 g/cm^3) and a massive presence of rock aggregate ($60.5 \pm 6.4\%$, Table 2), mainly consisting of local rhyodacite (2.60 g/cm^3) and granitoids (2.70 g/cm^3). In lime render, 39.4% of total aggregate is also represented by felsic crystal-clasts (with average density of 2.65 g/cm^3) and mafic crystal-clasts (0.1%) with opaque (> 5 g/cm^3; Klein 2004).

In finishing coat, the solid density is higher (2.71 ± 0.01 g/cm^3), because it is affected by a weak presence of aggregates (average $B/A = 5.38$, Table 3) and prevailing carbonate binder with a density of 2.70 g/cm^3.

Real density is correlated with closed porosity and shows values of 2.53 ± 0.06 g/cm^3 in *Trullissatio*, 2.64 ± 0.02 g/cm^3 in lime render and 2.66 ± 0.03 g/cm^3 in finishing coat (Fig. 7a, Table 6).

The highest total porosity (Fig. 7b) is detected in lime render ($41.2 \pm 6.5\%$), while lowest value is detected in *Trullissatio* ($37.3 \pm 3.8\%$).

As we can see from Fig. 7b, in *Trullissatio*, the total porosity is represented by $\approx 96\%$ of helium open porosity and $\approx 4\%$ of closed porosity. Similar configuration is recorded in lime renders with Φ_OHe $\approx 95\%$ of Φ_T and $\Phi_C \approx 5\%$ of Φ_T (Table 6). An average intermediate value of total porosity is recorded in the finishing coat with $38.9 \pm 5.8\%$, where Φ_OHe is $\approx 96\%$ of Φ_T and $\Phi_C \approx 4\%$ of Φ_T. As shown in Fig. 7, all the samples show following variation ranges of the saturation index (S.I.): $78.1 < $ S.I. $ < 98.6\%$, and imbibition coefficient (CI$_W$): $10.7 < $ CI$_w < 33.4\%$. Point load strength index of mortars (Table 7, Fig. 7d) ranging from 0.17 to 0.30 N/mm^2 and it is weakly correlated with void ratio (e) by a polynomial correlation ($R^2 \approx 0.2$).

Table 5 Particle size distribution (PSD) of mortar aggregates: midpoint passing diameters on 60–10% and coefficients of uniformity

Mortar	Function	Midpoint passing diameter on 60% $D_{60\%}$ (μm)	Midpoint passing diameter on 10% $D_{10\%}$ (μm)	Coefficient of uniformity U ($U = D_{60\%}$ / $D_{10\%}$)	Particle size typology according to U
FT48f	Ceramic fragments render (*Trullissatio*)	5000	340	14.7	Various
FT49f		5300	500	10.6	Various
FT50		1500	130	11.53	Various
FT52s		3000	240	12.5	Various
FT53s		900	80	11.25	Various
FT56a′		3600	250	14.4	Various
FT58a′		1900	230	8.26	Various
FT58a″		4000	250	16	Very various
FT37a	Lime render	700	290	2.41	Uniform
FT38a		700	290	2.41	Uniform
FT39a		1000	300	3.33	Uniform
FT40a		1100	270	4.07	Uniform
FT42f		850	300	2.83	Uniform
FT44f		1000	160	6.25	Various
FT46f		530	280	1.89	Uniform
FT54s		1800	120	15	Various
FT37b	Finishing coat	1700	300	5.66	Various
FT38b		1600	250	6.4	Various
FT39b		1000	280	3.57	Uniform
FT40b		1000	240	4.17	Uniform
FT43f		400	250	1.6	Uniform
FT45f		1600	370	4.32	Uniform
FT47f		1500	330	4.54	Uniform
FT55s		230	150	1.53	Uniform

pXRD diffraction on mortars

Table 8 exhibits the semi-quantitative mineralogical characterization of the powder mortars (by pXRD).

The analyses define a calcitic ($CaCO_3$) binder with quartz, plagioclase, K-feldspar and muscovite, sometimes present in traces (lime renders FT39a, FT40a) or abundant (FT46f, FT40b). These minerals represent the composition of the sands used as aggregate.

In samples FT58a′ and FT40a, chlorite is mainly due to devitrification mineral of cineritic groundmass in local rhyolites and rhyodacites used as rock aggregate (Sitzia 2019). The identified kaolinite derives from hydrolysis of plagioclase and K-feldspar (Mackenzie and Guilford 1980).

The provenience of sodium chloride (NaCl) found in the samples the FT48f and FT58a′ is uncertain. A first hypothesis is that it may derive from marine aerosol. As the monuments are about 30 km from the West coast, the occurrence of sea salt suspension is explained by the presence of prevalent strong winds coming from N-W quarter.

As we will see after, the presence of Cl-salts on the materials also could give to the evaporation of saline solutions formed by mixing of flood waters (from Tirso river) and thermal waters (Dettori et al. 1982) during flooding events. The sodium chloride could also derive from poor washing of the marine sandy aggregates used in mortars.

Thermal-gravimetric analysis on binders

The thermal decomposition curves of the mortars, shown in Fig. 8, present two characteristic weight losses.

A first weight loss is detected between 200 and 520 °C, due to the evaporation of chemical-physical bound water ($\Delta H_2O\%$) of hydraulic phases, such as calcium silicate (C–S–H) and calcium aluminate hydrates (C–A–H). A second weight loss is detected between 550 and 830 °C, due to the decarbonation of the binder ($\Delta CO_2\%$).

Both the two main weight losses are reported in Table 9 and shown in Fig. 8a, according to Moropoulou diagram (Moropoulou et al. 2005; Moropoulou et al. 2004; Moropoulou et al. 1995).
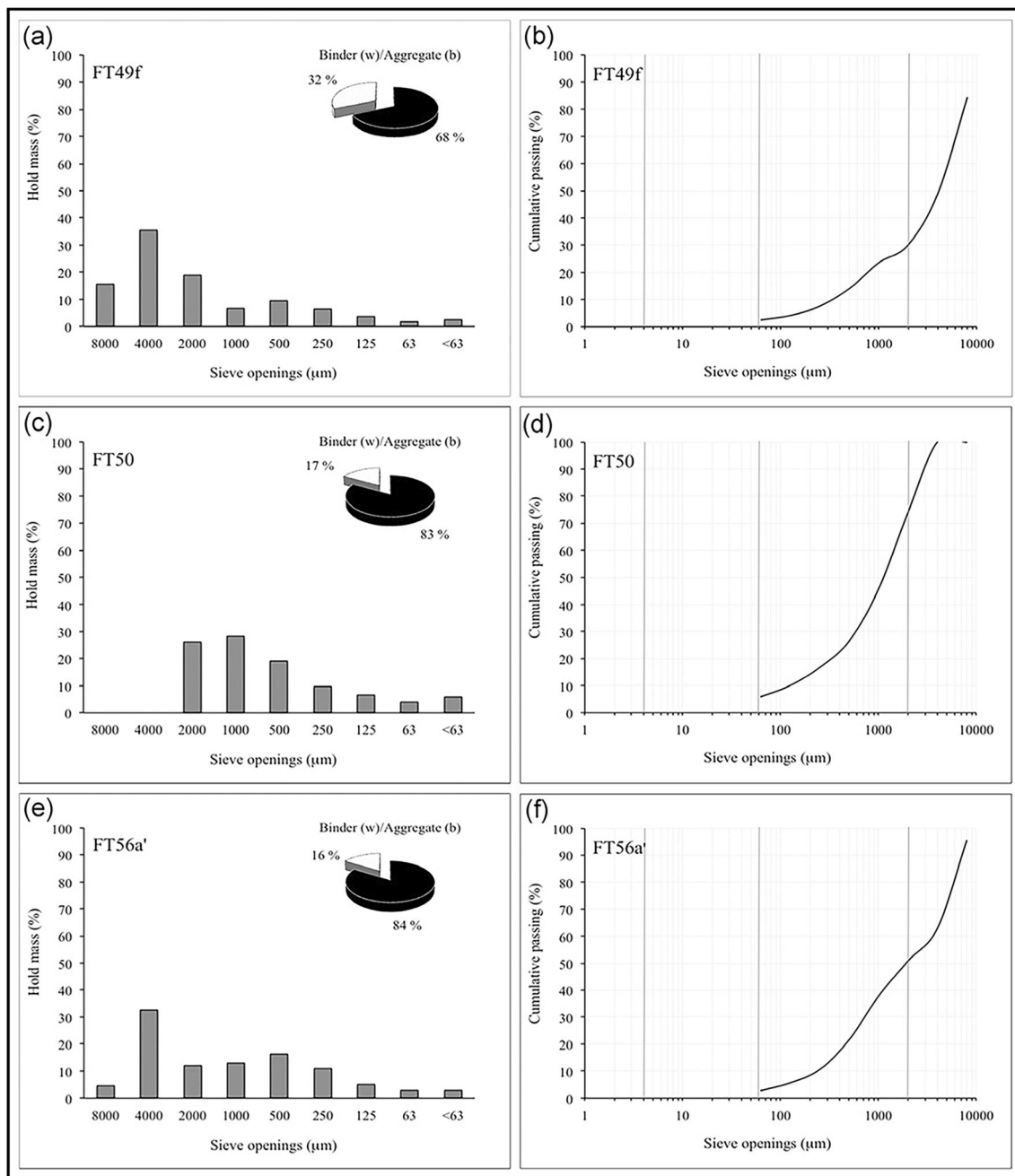
Fig. 5 Particle-size distribution PSD of mortar aggregates: **a**, **b** *Trullissatio* FT49f; **c**, **d** *Trullissatio* FT50; **e**, **f** *Trullissatio* FT56a′

As shown in Fig. 8a, the hydraulic degree of the mortars, inversely proportional with ΔCO_2, appears in the following order:

$\Delta CO_2 = 16.3 \pm 0.8\%$ in *Trullissatio*, $\Delta CO_2 = 20.6 \pm 2.6\%$ in finishing coat and $\Delta CO_2 = 22.1 \pm 1.0\%$ in lime render.

Considered the same calcitic composition of the binder in all the groups, in *Trullissatio* mortars, the high hydraulicity could be conferred by the ceramic fragment aggregates, with an average of $73.7 \pm 15.5\%$ (Table 2), which involves (by

reaction with the lime) the formation of C–S–H and C–A–H phases.

In finishing coat and lime render mortars, showing similar hydraulic degree, the different $\Delta CO_2/\Delta H_2O$ ratio (equal to $12.3 \pm 2.2\%$ and $21.7 \pm 2.9\%$ respectively), is due to a higher loss of water in finishing coat. In the group, the high dispersion of $\Delta CO_2\%$ values is due to the FT38b sample that shows a higher hydraulic degree than group average, moving away from polynomial trend line (Fig. 8a). This high hydraulicity of
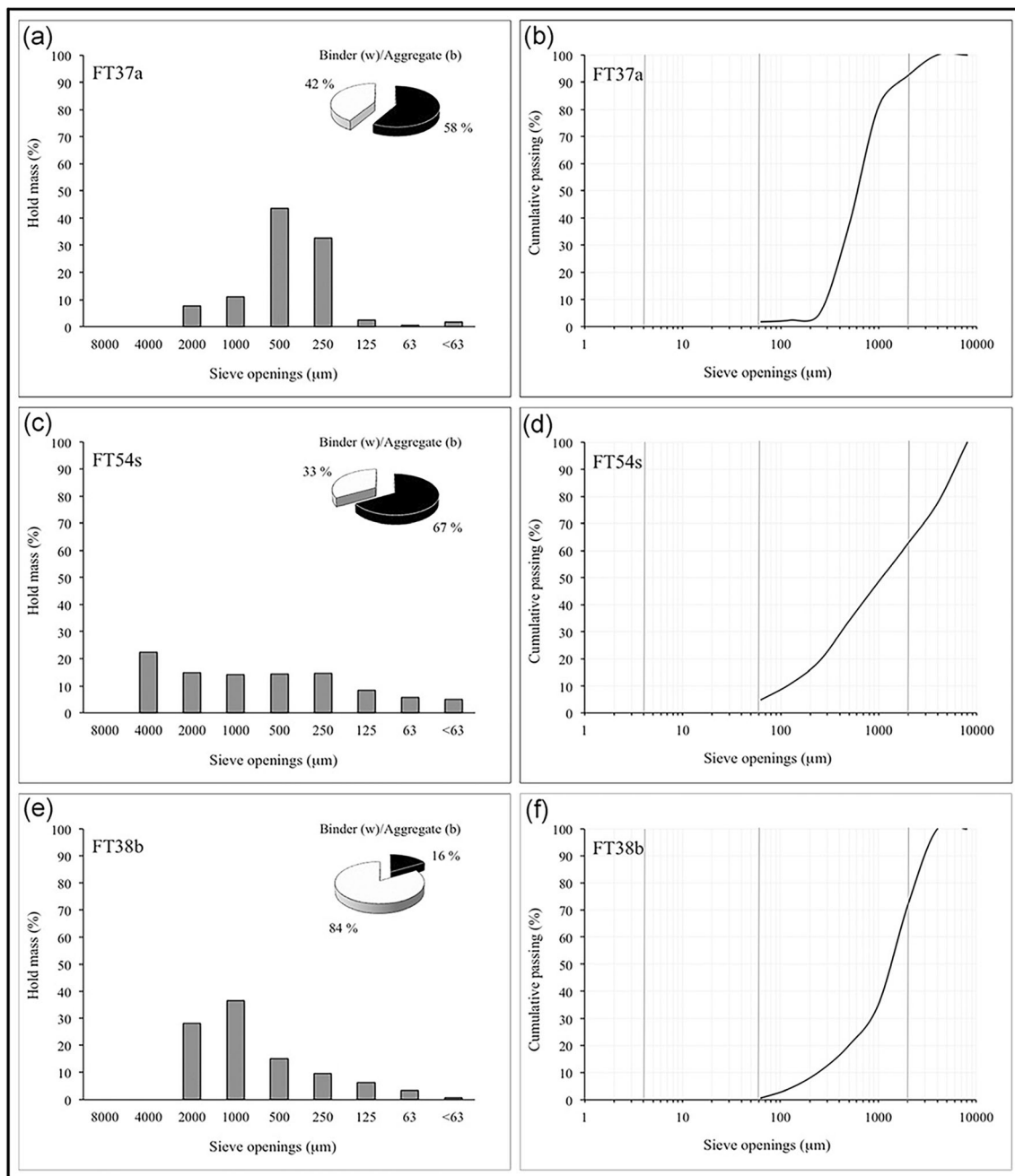
Fig. 6 Particle size distribution PSD of mortar aggregates: **a**, **b** lime render FT37a; **c**, **d** lime render FT54s; **e**, **f** finishing coat FT38b

FT38b could derive from a fragment of aggregate not correctly separated from the binder.

μ-XRD, μ-FTIR and μ-Raman on paintings

The results obtained by μ-XRD diffraction on paintings are presented in Table 10 and Fig. 9a–d, relative to samples FT39b and FT47f. In all cases, calcite was identified as primary component of the painted support. Other mineralogical phases like calcium-rich plagioclase, K-feldspars, quartz, pyroxene, rutile and muscovite-illite were included in the aggregate fraction. Nitratine and hydrocalumite are, respectively, surface efflorescence due to mortar humidity (Siedel 2018) and a reaction product between mortar gel C–A–H and Cl⁻ anions (Vola et al. 2011).

Finally, the red colour on the most of the samples was mainly due to iron oxides (most probably red ochre), considering the identification of haematite, while on orange samples, both haematite and goethite are identified like in other analytical works (Piovesan et al. 2011; Angelini et al. 2019). On one

Table 6 Physical characterization of mortars (italic differentiates standard deviations and arithmetic averages from the rest of the data)

Mortar	Function	In situ humidity	Solid density	Real density	Bulk density	Total porosity	Helium open porosity	Water open porosity	Closed porosity	Void ratio	Imbibition coefficient	Saturation index
		U (g/g)	ρ_S (g/cm³)	ρ_R (g/cm³)	ρ_B (g/cm³)	Φ_T (%)	Φ_{He} (%)	ΦH_2O (%)	Φ_C (%)	e ()	CI_w (%)	S.I. (%)
FT48f	Ceramic fragments render (*Trullissatio*)	0.01	2.66	2.61	1.52	43.6	41.7	33.9	1.8	0.76	22.3	81.3
FT49f		0.05	2.57	2.54	1.72	33.5	32.4	31.1	1.1	0.5	18.1	95.8
FT50		0.01	2.49	2.48	1.54	37.9	37.8	35.9	0.1	0.61	23.2	95
FT52s		0.01	2.5	2.47	1.62	35.9	34.3	30.7	1.5	0.56	18.9	89.3
FT53s		0.01	2.5	2.45	1.69	33.2	31.1	26.6	2.1	0.49	15.8	85.6
FT56a′		0.01	2.55	2.51	1.56	39.3	37.6	33.9	1.7	0.64	21.7	90.2
FT58a′		0.02	2.59	2.55	1.53	41.3	40	36.1	1.3	0.7	23.6	90.4
FT58a″		0.03	2.66	2.59	1.77	34.	31.5	24.6	2.5	0.51	13.8	78.2
Arithmetic average		*0.02*	*2.56*	*2.53*	*1.62*	*37.3*	*35.8*	*31.6*	*1.5*	*0.6*	*19.7*	*88.2*
Standard deviation		*0.02*	*0.07*	*0.06*	*0.1*	*3.8*	*4.0*	*4.2*	*0.7*	*0.1*	*3.6*	*6.1*
FT37a	Lime render	0.01	2.71	2.65	1.44	48.1	45.6	43.1	2.4	0.91	30	94.5
FT38a		0.03	2.69	2.64	1.82	32.8	31.2	30.1	1.6	0.49	16.5	96.5
FT39a		0.09	2.65	2.61	1.37	48.9	47.4	45.9	1.4	0.95	33.4	96.7
FT40a		0.05	2.68	2.65	1.57	42.1	40.9	37.5	1.2	0.72	23.9	91.5
FT42f		0.1	2.72	2.67	1.63	40.8	39	31.1	1.7	0.68	19.1	79.7
FT44f		0.06	2.65	2.61	1.6	40	38.7	36.4	1.2	0.66	22.8	94
FT46f		0.01	2.73	2.64	1.9	31.2	27.8	26	3.4	0.45	13.6	93.7
FT54s		0.01	2.67	2.65	1.46	45.7	44.8	39.7	0.8	0.84	27.2	88.5
Arithmetic average		*0.05*	*2.69*	*2.64*	*1.6*	*41.2*	*39.4*	*36.2*	*1.7*	*0.71*	*23.3*	*91.9*
Standard deviation		*0.04*	*0.03*	*0.02*	*0.18*	*6.5*	*6.9*	*6.7*	*0.8*	*0.18*	*6.7*	*5.5*
FT37b	Finishing coat	0.06	2.7	2.65	1.59	41.8	40.1	37.4	1.6	0.71	23.5	93.1
FT38b		0.03	2.72	2.67	1.77	35.5	33.4	32.4	2	0.54	18.2	96.9
FT39b		0.05	2.7	2.62	1.54	44.2	41	40.4	3.1	0.77	26.2	98.6
FT40b		0.01	2.71	2.62	1.54	44.4	41.1	33.6	3.2	0.78	21.8	81.9
FT43f		0.03	2.71	2.7	1.61	40.7	40.1	31.6	0.6	0.69	19.6	78.9
FT45f		0.01	2.69	2.66	1.61	40.4	39.4	38.2	1	0.67	23.7	97.1
FT47f		0.01	2.71	2.69	1.99	26.6	26.1	21.2	0.4	0.36	10.7	81.2
FT55s		0.02	2.72	2.68	1.7	37.9	36.7	28.7	1.2	0.61	16.9	78.1
Arithmetic average		*0.03*	*2.71*	*2.66*	*1.67*	*38.9*	*37.2*	*32.9*	*1.6*	*0.64*	*20.1*	*88.2*
Standard deviation		*0.02*	*0.01*	*0.03*	*0.15*	*5.8*	*5.1*	*6.1*	*1*	*0.14*	*4.9*	*8.9*

black sample, neither iron or manganese oxides were detected suggesting the utilization of charcoals for this colour.

The analysis µ-FTIR of eight micro-samples selected for this study reflected a consistency in the orange paint compositions. Figure 9e presents a representative spectrum of the results, where it was possible to identify some of the characteristic absorption bands of silicates (namely the strong absorption band at 1042 cm^{-1} peak is related to Si–O stretching) and of calcium carbonates (specifically the absorption bands at 1795, 1405 due to the ν (CO_3^{2-}) stretching and the sharp picks at 872 and 711 cm^{-1} related to the δ (CO_3^{2-}) (Saǧin et al. 2012). The weak absorption band at 1741 cm^{-1} that can be attributed to the carbonyl stretching of the ester ν(C=O) of oxidized triglycerides and the shoulder at 1640 cm^{-1} that

can be related to the Amide I ν(C=O) stretching, together with the and the CH's absorption band's profile from the fatty acid chain due to the methylene stretching groups at circa 2982 and 2873 cm^{-1} suggest the presence of a strongly oxidized tempera as binding medium (Miguel et al. 2012).

All the results obtained by Raman microscopy are similar to those obtained by other analytical works carried out on Roman wall paintings (Aliatis et al. 2010; Baraldi et al. 2007; Gutman et al. 2016; Angelini et al. 2019). As example, we report spectra from samples FT39b (orange) and FT47f (red) (Fig. 9f, g). Calcite bands 230, 282, 717 and 1087 cm^{-1} were identified in the most of the samples. Red samples are characterized by the presence of haematite, with its characteristic Raman bands at 225, 288, 407, 493, 606, 652 and 1315 cm^{-1}, while in orange

Table 7 Mechanical characterization of mortars (italic differentiates standard deviations and arithmetic averages from the rest of the data)

Mortar	Function	Point load strength index Is_{50} (N/mm^2)	Compressive strength R_C (N/mm^2)	Tensile strength R_T (N/mm^2)
FT48f	Ceramic fragments render (*Trullissatio*)	0.53	7.42	0.66
FT49f		0.75	10.44	0.93
FT50		1.04	14.59	1.3
FT52s		0.83	11.6	1.04
FT53s		0.54	7.55	0.67
FT56a′		0.41	5.71	0.51
FT58a′		0.37	5.23	0.47
FT58a″		0.38	5.37	0.48
Arithmetic average		*0.61*	*8.61*	*0.77*
Standard deviation		*0.23*	*3.2*	*0.29*
FT37a	Lime render	0.44	6.12	0.55
FT38a		0.29	4.03	0.36
FT39a		0.25	3.5	0.31
FT40a		0.14	1.92	0.17
FT42f		0.59	8.31	0.74
FT44f		0.42	5.88	0.52
FT46f		0.61	8.53	0.76
FT54s		0.34	4.76	0.43
Arithmetic average		*0.39*	*5.5*	*0.49*
Standard deviation		*0.15*	*2.06*	*0.18*
FT37b	Finishing coat	0.38	5.32	0.48
FT38b		0.4	5.6	0.5
FT39b		0.38	5.39	0.48
FT40b		0.35	4.93	0.44
FT43f		0.4	5.6	0.5
FT45f		0.38	5.27	0.47
FT47f		0.5	7	0.63
FT55s		0.48	6.76	0.6
Arithmetic average		*0.39*	*5.41*	*0.48*
Standard deviation		*0.09*	*1.19*	*0.11*

samples, both characteristic Raman bands of haematite and goethite at 302, 386 and 476 cm^{-1} were identified, as previously observed during μ-XRD analyses.

Discussion of results

The archaeometric investigations allow us to recognize the technological choices done by the Roman builders in *Forum Traiani* baths in the production of mortars.

The wall plaster generally consists of three main layers of mortars rather ceramic fragment renders (*Trullissatio*), lime renders and finishing coat. The *Trullissatio* layers, due to the high degree of hydraulicity, performs a waterproofing function, while the lime render mortar was a preparation layer for the finishing coat. On this, red, orange and black artistic paintings were applied using pigments like haematite Fe_2O_3 (for the red colour), goethite FeO (OH) (for orange) and probably charcoal (for black). The μ-FTIR results suggest the use of tempera as binding medium for wall paintings.

The OM observations on ceramic fragments temper from *Trullissatio* mortars highlight the use of various type of pottery (e.g. bricks, tiles and probably wheel made ceramics). The results show a double source of raw materials used for the rock aggregate. The rock rubble employed in the mortars, mainly represented by well-rounded fragments of local rhyolites and rhyodacites, indicate a probable origin from Tirso riverbed. However, the presence of bioclasts characterized by marine fossil fauna (e.g. echinoderm and coralline algae) also highlights the use of marine sand.

In some samples, the selection degree of aggregates and ceramic fragments presence causes slight particle size gaps.
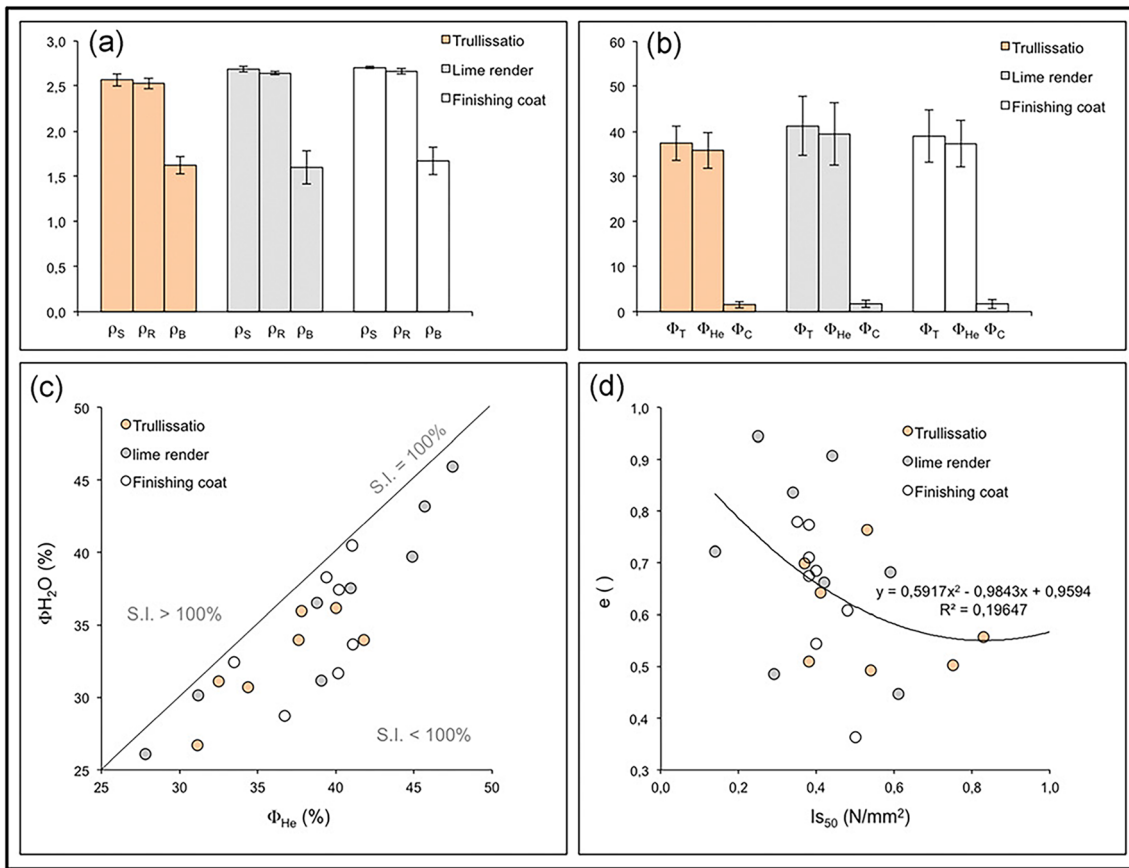
Fig. 7 Physical-mechanical characterization of mortars: **a** histogram of mortar average densities with standard deviations: ρ_S, solid density; ρ_R, real density; ρ_B, bulk density; **b** histogram of mortar average porosities with standard deviations: Φ_{He}, helium open porosity; Φ_T, total porosity; Φ_C, closed porosity; **c** helium open porosity (Φ_{He}) vs water open porosity(ΦH_2O); **d** Point load strength index (Is_{50}) vs void ratio (e)

The result is a different aggregate PSD in *Trullissatio* and mainly uniform PSD in lime renders and finishing coat. The use of different aggregates sizes was recommended by Vitruvius, because it allows to save binder and to increase the mechanical strength, as demonstrate by the values of point load, tensile and compression. In *Trullissatio*, the high values of mechanical strength are also confirmed by the greater hydraulicity of binder.

Macroscopic and OM observations on mortars proved the presence of a fracturing system, probably due to degradation caused by the presence of sodium chloride and consequently hydrocalumite. The origin of this phase is probably the poor

Table 8 Diffraction (pXRD) on mortars: *Ca*, calcite; *Qz*, quartz; *Pla*, plagioclase; *Kf*, K-feldspar; *Mu*, muscovite; *Chl*, chlorite; *Kao*, kaolinite, *Ill*, illite; *Ha*, halite; *Tr*, traces (≤ 2% wt.), "•" indicates present (2–10% wt.), "••" indicates abundant (10–40% wt.) and "•••" indicates very abundant (≥ 40% wt.)

Mortar	Function	Ca	Qz	Pla	Kf	Mu	Chl	Kao	Ill	Ha
FT48f	Ceramic fragments render (*Trullissatio*)	•••	••	•	-	•	-	-	-	Tr
FT49f		•••	••	•	•	-	-	-	Tr	-
FT56a′		•••	•	••	-	••	-	-	-	–
FT58a′		•••	••	-	-	-	Tr	-	Tr	Tr
FT39a	Lime render	•••	••	•	•	Tr	-	•	Tr	-
FT40a		•••	••	•	-	Tr	Tr	-	-	-
FT46f		•••	Tr	••	••	••	-	••	-	-
FT54s		•••	Tr	••	•	-	-	-	-	-
FT37b	Finishing coat	•••	Tr	-	-	-	-	-	-	-
FT38b		•••	••	•	•	-	-	•	Tr	-
FT39b		•••	••	•	•	-	-	-	-	-
FT40b		•••	••	•	-	•	-	•	-	-
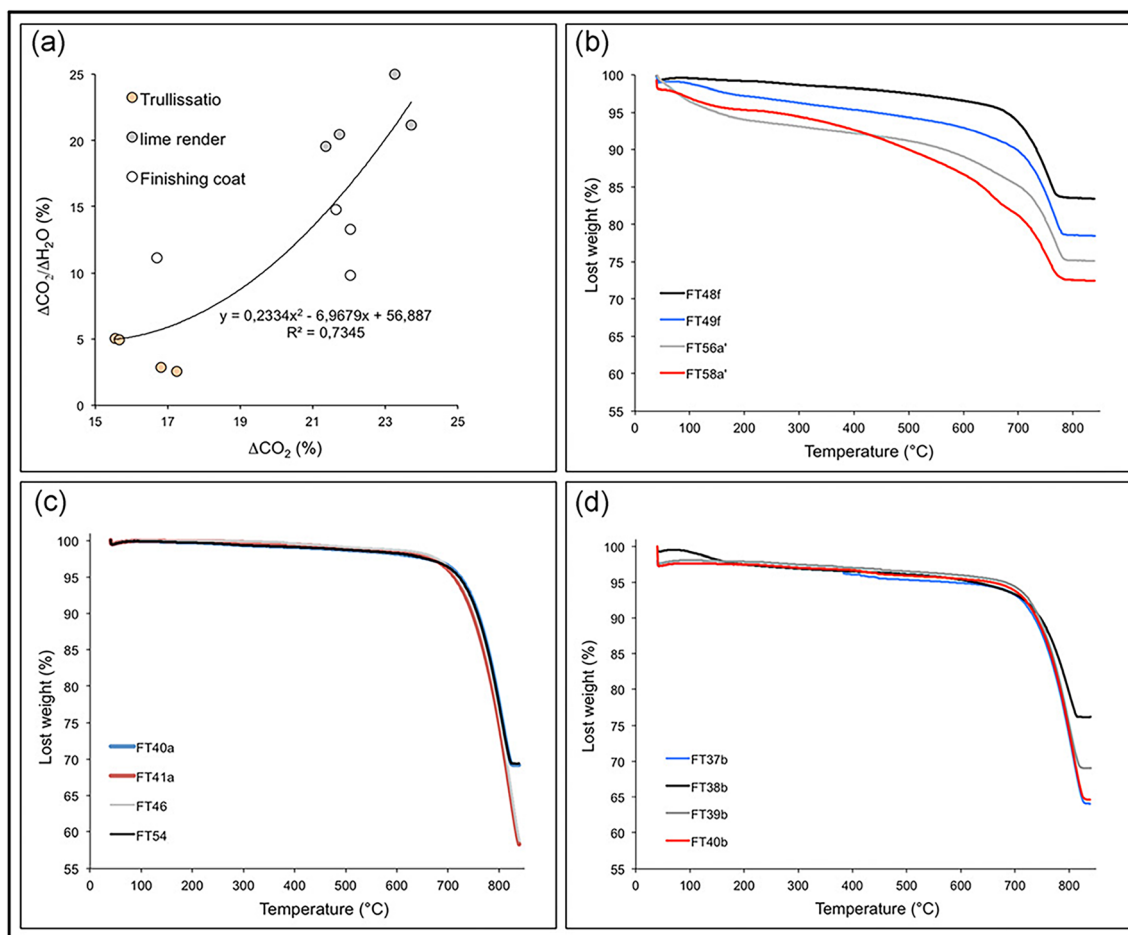
Fig. 8 Thermal characterization of mortars: **a** ΔCO_2 vs $\Delta CO_2/\Delta H_2O$ diagram, **b** thermal decomposition curves of ceramic fragment renders (*Trullissatio*), **c** thermal decomposition curves of lime renders, **d** thermal decomposition curves of finishing coats

washing of the marine sands or contamination by the thermal NaCl-bearing waters today still flowing in the archaeological site. The washing of aggregates from marine sodium chloride was a fundamental step already described by Vitruvius in 15 BC. The presence of NaCl in the sandy aggregates could cause alterations of the standard mortar setting times and more serious damage into the masonry.

The study of the mortar stratigraphy series (f) (Fig. 10) from *Frigidarium* "n" room highlights the presence of three alternations of lime renders-finishing coat and two *Trullissatio* layers. This series is extremely important in the analysis of some aspects related to the construction stages of the *Frigidarium* ("n" room in Fig. 2). In the first (I) plaster cycle (Fig. 10), the finishing coat presents a fresco surface (A-A′). The second (II) and third (III) plaster cycles with relative painting surfaces (B-B′ and C-C′) were subsequently realized on the first one (Fig. 10). The II and III cycles probably were restoration interventions. Deterioration of plasters and paintings could be caused by the presence of humidity in the room or by the flooding of the Tirso. In fact, the hydrogeological risks in *Forum Traiani* area is high (Hi1 and Hi4 degree; PAI, Piano di assetto idrogeologico regione Sardegna), due to

events of flooding with return time on average 50 years. These important hydrological events have undoubtedly affected the various rooms of the baths, involving the circulation of saline aqueous solutions within the materials. In these solutions, salt came from the soil and from the construction materials themselves (especially mortars).

The two last *Trullissatio* layers highlight the presence of other two plaster cycles (IV and V), considering their different composition, thickness, grain-size and not standard laying sequence. This probably indicates the attempt to create a definitive waterproofing for two times or, in any case, a mechanically strong layer ceramic fragments-bearing.

Moreover, to confirm this evidence, it is absolutely indicative that the only finishing coats (some of which are still frescoed) that can be seen today in the archaeological area are located in the *housing structures*, positioned at higher altitudes, where hydrogeological risk is lower (Hi1) respect than the *Frigidarium* and *Natatio* ground levels which have a higher risk (Hi4). A significant discussion about the technological meaning of these two different layers over three plaster cycles can be done. Considered the flooding events certainly occurred in the archaeological site during four centuries (I–IV

Table 9 Thermal characterization (TGA) on binders (italic differentiates standard deviations and arithmetic averages from the rest of the data)

Function		Weight lost in temperature ranges (%)		$\Delta CO_2/\Delta H_2O$
		200–520 °C (ΔH_2O)	520–800 °C (ΔCO_2)	
FT48f	Ceramic fragments render (*Trullissatio*)	6.72	17.24	2.56
FT49f		3.09	15.56	5.04
FT56a′		3.17	15.66	4.95
FT58a′		5.94	16.81	2.83
Arithmetic average		*4.73*	*16.32*	*3.84*
Standard deviation		*1.88*	*0.84*	*1.33*
FT39a	Lime render	1.12	23.71	21.17
FT40a		1.09	21.37	19.53
FT46f		0.93	23.27	24.98
FT54s		1.06	21.73	20.46
Arithmetic average		*1.03*	*22.12*	*21.66*
Standard deviation		*0.09*	*1.01*	*2.92*
FT37b	Finishing coat	2.24	22.04	9.82
FT38b		1.49	16.7	11.17
FT39b		1.46	21.63	14.79
FT40b		1.66	22.04	13.31
Arithmetic average		*1.71*	*20.6*	*12.27*
Standard deviation		*0.36*	*2.61*	*2.21*

Cent. AD), it is probable that Romans had to provide two restoration interventions on the various rooms of the thermal baths. This is also confirmed by the presence of at least three plaster cycles in the square section pillars in the barrel roof above the *Natatio* (see Fig. 1b). The best observable wall mortar stratigraphy in the *Natatio* room consists (form inside to outside) of a ceramic fragments renders (8–10 mm), two different finishing coats (about 5–6 mm) belonging to first two cycles, and other two layers of last cycle, consisting of a ceramic fragment renders and a finishing coat.

These interventions, dated back between third and the first half of the fourth century, were cited in an epigraphic text, found in the baths during the excavations of 1990s and now lost (Serra and Bacco 2014). The inscription, object of re-examination in recent times, has been reported by a *Servus*

Publicus which, during I Cent. AD was the author of unspecified works inside the thermal baths (Serra and Bacco 2014).

The second stratigraphic series (s) (Fig. 11) collected in a water tank offers interesting informations about the Roman waterproofing methods. The results highlight the presence of two layers of *Trullissatio* mortars (samples FT52s, FT53s), a lime renders (FT54s) and a finishing coat (FT55s). In this case, Roman production technology can be especially observed in Binder/Aggregate (*B/A*) ratio and in particle-size distribution (PSD). In fact, in the mortar layers, a progressive increase of *B/A* ratio and a decrease of aggregate average size (Fig. 11) were observed from inside to outside. Thus, *Trullissatio* samples (FT52s, FT53s) show a *B/A* ratio of 0.23 and 0.66, respectively with different PSD ($d_H = 2000$–4000 μm in FT52s and 2000–500 μm (bimodal) in FT53s).

Table 10 Micro-diffraction (μ-XRD) results of pigments. *Ca*, calcite; *Nit*, nitratine; *Pla*, plagioclase; *Kf*, K-feldspar; *Qz*, quartz; *Prx*, pyroxene; *Mu/Ill*, muscovite/Illite; *Hm*, haematite; *Liz*, lizardite; *Ru*, rutile; *Go*, goethite; *Hy*, hydrocalumite; *Tr*, traces (≤ 2% wt.), "•" indicates present (2–10% wt.), "••"indicates abundant (10–40% wt.) and "•••"indicates very abundant (≥ 40% wt.)

Mortar	Pigment colour	Ca	Nit	Pla	Kf	Qz	Prx	Mu/Ill	Hm	Liz	Ru	Go	Hy
FT37b	Red	•	••	•••	-	Tr	•	-	-	-	-	-	-
FT38b	Red	••	-	•	-	•	-	•	Tr	Tr	-	-	-
FT39b	Orange	••	-	•	•	•	-	•	Tr	Tr	-	Tr	-
FT40b	Orange	•••	•	-	-	Tr	-	Tr	Tr	-	Tr	Tr	-
FT41b	Red	•••	-	•	-	Tr	-	•	Tr	-	-	-	-
FT43f	Black	••	••	•	-	Tr	-	-	-	-	Tr	-	-
FT43f	Red	•	•••	•	•	Tr	•	-	-	-	-	-	-
FT47f	Red	••	•••	•	-	Tr	Tr	-	Tr	-	-	-	Tr
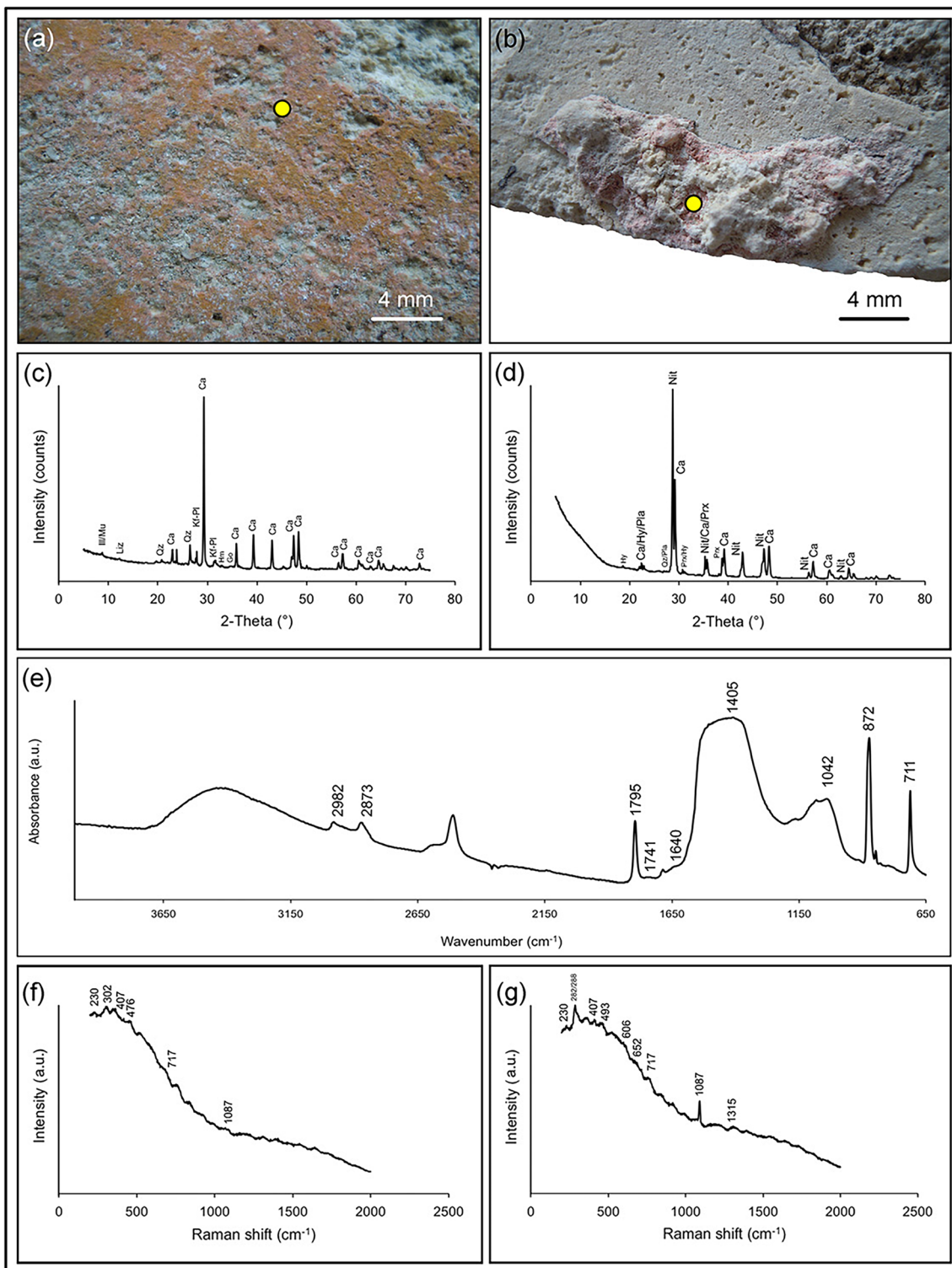
Fig. 9 Paintings characterization: **a** FT39b painting with analysis point, **b** FT47f painting with analysis point, **c** μ-XRD characterization on FT39b, **d** μ-XRD characterization on FT47f, **e** representative spectrum of the μ- FTIR results, **f** μ-Raman characterization on FT39b, **g** μ-Raman characterization on FT47f

The render sample (FT54s) shows a higher B/A ratio (0.48) with various PSD. The finishing coat FT55s, last of the waterproofing layer sequence, presents higher B/A (18.92) with medium size sand aggregate.

Conclusions

The research firstly allowed to focuses on technologies and production of plaster.

Fig. 10 First stratigraphic series of mortars (f): ρ_S, solid density; Φ_T, total porosity; Is_{50}, point load strength index; B/A, binder/aggregate ratio; d_H, sieve openings with maximum hold mass; U, coefficient of uniformity; A-A′, B-B′, C-C′, painted surfaces. Graphic processing by Fabio Sitzia
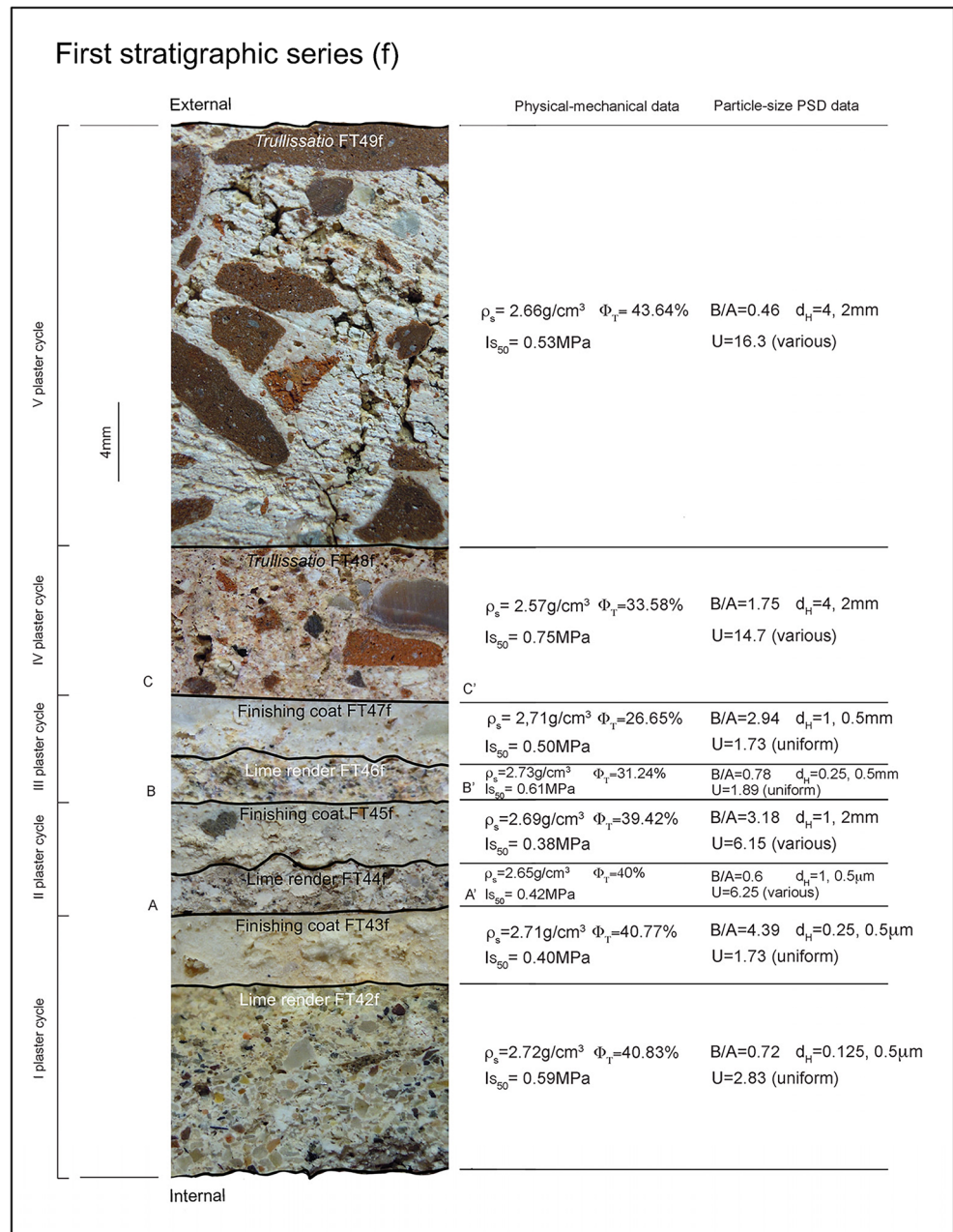
Moreover, by the detailed compositional study of some main complex stratigraphies of wall mortars (up to about 10 cm), it was also possible to observe the adopted technologies for the laying of numerous plaster cycles, highlighting the presence of ancient restoration interventions.

In the masonry walls, three main types of mortars with different compositions were used according to their function in the building: *Trullissatio*, lime renders and finishing coats. *Trullissatio* was used in high humidity environments (e.g. *Frigidarium* tank) and (as a "scratch coat" layer) to improve the adhesion between stone masonry or brick and the subsequent render. These mortars are generally less porous than the other mortars and are characterized by a variable binder/aggregate ratio inversely related to the mortar thickness. The hydraulicity of these mortars is conferred by fragments of ceramic, local rhyolite and rhyodacite of fluvial environment and crystal-clasts of marine origin.

Thanks to the presence of amorphous reactive glass phases, these volcanic rocks in turn have conferred an additional hydraulicity.

As for the plasters of the internal walls, in lime renders, a lime-based binder was used. These mortars present a quartz-feldspar sand of marine origin and, also in this case, fragments of local rhyolites and rhyodacites. These mortars, due to their carbonate composition and consequent low durability, have

Fig. 11 Second stratigraphic series of mortars (s): ρ_S, solid density; Φ_T, total porosity; Is_{50}, point load strength index; B/A, binder/aggregate ratio; d_H, sieves openings with maximum hold mass; U, coefficient of uniformity. Graphic processing by Fabio Sitzia
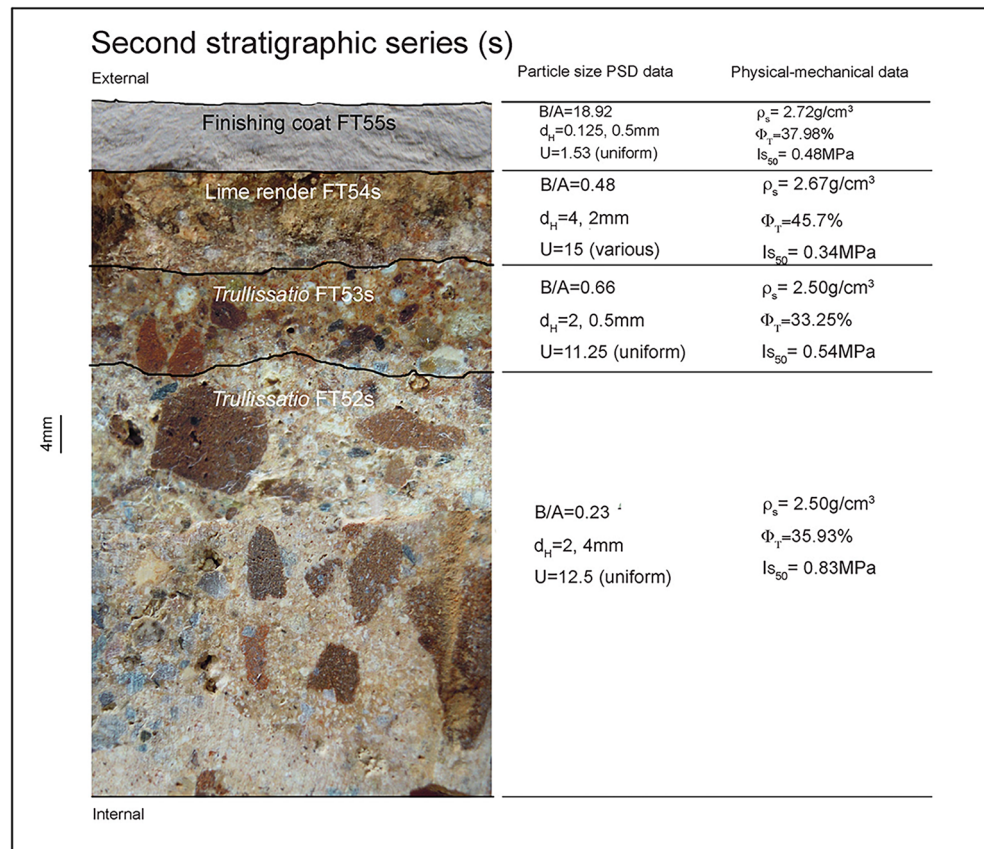
only been found in "n" *Frigidarium* room because they are covered by two layers of external Trullissatio that have preserved them, and in *housing structures* U (Fig. 2). The finishing coats were made according to the standards of the Roman period, using washed and selected aggregate, consisting of fine quartz-feldspar sand and subordinately fragments of volcanic rocks. Due to their high open He porosity and an easier absorption of CO_2 giving a high carbonation degree of binder, the finishing coats, as well as the renders, show a sufficient mechanical strength, comparable with the other mortars. The stratigraphies of mortars sampled in the *Frigidarium* and *Natatio* rooms, characterized in both cases by three plaster cycles, highlight the presence of different restoration interventions during Roman times. The *Natatio* presents restructuring interventions also in the steps, and in the floor. Restoring probably indicates a continuous degradation of building materials, induced both by the constant presence of humidity, but also certainly by the cyclic overflows of the Tirso.

References

Aliatis I, Bersani D, Campani E, Casoli A, Lottici PP, Mantovan S, Marino IG (2010) Pigments used in Roman wall paintings in the Vesuvian area. J Raman Spectrosc 41:1537–1542. https://doi.org/10.1002/jrs.2701

Angelini I, Asscher Y, Secco M, Parisatto M, Artioli G (2019) The pigments of the frigidarium in the Sarno Baths, Pompeii: identification, stratigraphy and weathering. J Cult Herit 40:309–316. https://doi.org/10.1016/j.culher.2019.04.021

Angiolillo S (1998) L'arte della Sardegna romana. Milano, Jaca Book

Antonelli F, Columbu S, De Vos RM, Andreoli M (2014) An archaeometric contribution to the study of ancient millstones from the Mulargia area (Sardinia, Italy) through new analytical data on volcanic raw material and archaeological items from Hellenistic and Roman North Africa. J Archaeol Sci 50:243–261

Argiolas S (2006) Caratterizzazione tecnologica e durevolezza di alcune piroclastiti Sarde: riflessi sui loro possibili impieghi in edilizia. Tesi di Dottorato di Ricerca in Ingegneria del Territorio, Università di Cagliari

Baraldi P, Baraldi C, Curina R, Tassi L, Zannini P (2007) A micro-Raman archaeometric approach to Roman wall paintings. Vib Spectrosc 43:420–426. https://doi.org/10.1016/j.vibspec.2006.04.029

Cagnana A (2000) Archeologia dei materiali da costruzione. SAP Società Archeologica S.r.l, Mantova

Cardoso I, Macedo MF, Vermeulen F, Corsi C, Santos Silva A, Rosado L, Candeias A, Mirao J (2014) A multidisciplinary approach to the study of archaeological mortars from the town of Ammaia in the Roman Province of Lusitania (Portugal). Archaeometry. 56:1–24. https://doi.org/10.1111/arcm.12020

Cennini C (1859) Il libro dell'arte. Le Monnier, Firenze

CNR–ICR (1980) Raccomandazione Nor.Ma.L 3/80: Materiali lapidei: campionamento, Rome

Columbu S (2017) Provenance and alteration of pyroclastic rocks from the Romanesque Churches of Logudoro (North Sardinia, Italy) using a petrographic and geochemical statistical approach. Appl

Phys A Mater Sci Process. https://doi.org/10.1007/s00339-017-0790-z

Columbu S (2018) Petrographic and geochemical investigations on the volcanic rocks used in the Punic-Roman archaeological site of Nora (Sardinia, Italy). Environ Earth Sci 77. https://doi.org/10.1007/s12665-018-7744-4

Columbu S, Garau AM (2017) Mineralogical, petrographic and chemical analysis of geomaterials used in the mortars of Roman Nora theatre (South Sardinia, Italy). Ital J Geosci 136:238–262. https://doi.org/10.3301/IJG.2017.05

Columbu S, Sitzia F, Verdiani G (2015) Contribution of petrophysical analysis and 3D digital survey in the archaeometric investigations of the Emperor Hadrian's Baths (Tivoli, Italy). Rend Lincei 26:455–474. https://doi.org/10.1007/s12210-015-0469-3

Columbu S, Sitzia F, Ennas G (2016) The ancient pozzolanic mortars and concretes of Heliocaminus baths in Hadrian's Villa (Tivoli, Italy). Archaeol Anthropol Sci 9:523–553. https://doi.org/10.1007/s12520-016-0385-1

Columbu S, Lisci C, Sitzia F, Buccellato G (2017) Physical-mechanical consolidation and protection of Miocenic limestone used on Mediterranean historical monuments: the case study of Pietra Cantone (Southern Sardinia, Italy). Environ Earth Sci 76. https://doi.org/10.1007/s12665-017-6455-6

Columbu S, Lisci C, Sitzia F, Lorenzetti G, Lezzerini M, Pagnotta S, Raneri S, Legnaioli S, Palleschi V, Gallello G, Adembri B (2018a) Mineralogical, petrographic and physical-mechanical study of Roman construction materials from the Maritime Theatre of Hadrian's Villa (Rome, Italy). Meas J Int Meas Confed 127:264–276. https://doi.org/10.1016/j.measurement.2018.05.103

Columbu S, Piras G, Sitzia F, Pagnotta S, Raneri S, Legnaioli S, Palleschi V, Lezzerini M, Giamello M (2018b) Petrographic and mineralogical characterization of volcanic rocks and surface-depositions on Romanesque monuments. Mediter Archaeol Archaeom. https://doi.org/10.5281/zenodo.1256051

Columbu S, Palomba M, Sitzia F, Murgia MR (2018c) Geochemical, mineral-petrographic and physical-mechanical characterization of stones and mortars from the Romanesque Saccargia Basilica (Sardinia, Italy) to define their origin and alteration. Ital J Geosci 137:369–695. https://doi.org/10.3301/IJG.2018.04

Columbu S, Antonelli F, Sitzia F (2018d) Origin of Roman worked stones from St. Saturno Christian Basilica (South Sardinia, Italy). Mediterranean Archaeology and Archaeometry. https://doi.org/10.5281/zenodo.1256047

Columbu S, Carboni S, Pagnotta S, Lezzerini M, Raneri S, Legnaioli S, Palleschi V, Usai A (2018e) Laser-induced breakdown spectroscopy analysis of the limestone Nuragic statues from Mont'e Prama site (Sardinia, Italy). Spectrochim Acta B At Spectrosc 149:62–70. https://doi.org/10.1016/j.sab.2018.07.011

Columbu S, Garau AM, Lugliè C (2019a) Geochemical characterisation of pozzolanic obsidian glasses used in the ancient mortars of Nora Roman theatre (Sardinia, Italy): provenance of raw materials and historical–archaeological implications. Archaeol Anthropol Sci 11:2121–2150. https://doi.org/10.1007/s12520-018-0658-y

Columbu S, Gioncada A, Lezzerini M, Sitzia F (2019b) Mineralogical-chemical alteration and origin of Ignimbritic stones used in the Old Cathedral of Nostra Signora di Castro (Sardinia, Italy). Stud Conserv 64:397–422. https://doi.org/10.1080/00393630.2018.1565016

Dettori B, Zanzari RA, Zuddas P (1982) Le acque termali della Sardegna. PFE Sottoprogetto Energia Geotermica. Relazione finale sul tema della ricerca: Studi geologici e geofisici finalizzati alla ricerca di fluidi caldi nel sottosuolo. Istituto di Geopedologia – Geologia applicata, Univerità di Sassari

Franklin JA (1985) Suggested method for determining point load strength. Int J Rock Mech Min Sci 22:51–60. https://doi.org/10.1016/0148-9062(85)92327-7

Gutman M, Zanier K, Lux J, Kramar S (2016) Pigment analysis of roman wall paintings from two villae rusticae in Slovenia. Mediter Archaeol Archaeom. https://doi.org/10.5281/zenodo.160970

Il territorio in epoca romana

Jackson MD, Chae SR, Mulcahy SR, Meral C, Taylor R, Li P, Emwas AH, Moon J, Yoon S, Vola G, Wenk HR, Monteiro PJM (2013) Unlocking the secrets of Al-tobermorite in Roman seawater concrete. Am Mineral 98:1669–1687. https://doi.org/10.2138/am.2013.4484

Klein C (2004) Mineralogia. Zanichelli, Bologna

Krumbein WC (1941) Measurement and geological significance of shape and roundness of sedimentary particles. J Sediment Res 11(2):64–72

Lafuente B, Downs RT, Yang H, Stone N (2016) The power of databases: the RRUFF project. Highlights in Mineralogical Crystallography. https://doi.org/10.1515/9783110417104-003

Lezzerini M, Antonelli F, Columbu S, Gadducci R, Marradi A, Miriello D, Parodi L, Secchiari L, Lazzeri A (2016, 2014) Cultural heritage documentation and conservation: three-dimensional (3D) laser scanning and geographical information system (GIS) techniques for thematic mapping of facade stonework of St. Nicholas Church (Pisa, Italy). International Journal of Architectural Heritage. https://doi.org/10.1080/15583058.2014.924605

Lezzerini M, Raneri S, Pagnotta S, Columbu S, Gallello G (2018) Archaeometric study of mortars from the Pisa's Cathedral Square (Italy). https://doi.org/10.1016/j.measurement.05.057

Mackenzie WS, Guilford C (1980) Atlas of rock-forming minerals in thin section. Mineral Mag

Mastino A (2005) La storia della Sardegna antica, Nuoro. Il Maestrale, Nuoro

Meloni P (1990) La provincia di Oristano, l'orma della storia. Pizzi, Milano

Miguel C, Lopes JA, Clarke M, Melo MJ (2012) Combining infrared spectroscopy with chemometric analysis for the characterization of proteinaceous binders in medieval paints. Chemom Intell Lab Syst 119:32–38. https://doi.org/10.1016/j.chemolab.2012.09.003

Miriello D, Antonelli F, Apollaro C, Bloise A, Bruno N, Catalano M, Columbu S, Crisci G. M, De Luca R, Lezzerini M, Mancuso S, La Marca A (2015) A petro-chemical study of ancient mortars from the archaeological site of Kyme (Turkey). Periodico di Mineralogia https://doi.org/10.2451/2015PM0028

Miriello D, Antonelli F, Bloise A, Ceci M, Columbu S, De Luca R, Lezzerini M, Pecci A, Mollo BS, Brocato P (2019) Archaeometric approach for studying architectural earthenwares from the archaeological site of St. Omobono (Rome-Italy) 9. https://doi.org/10.3390/min9050266

Moropoulou A, Bakolas A, Bisbikou K (1995) Characterization of ancient, byzantine and later historic mortars by thermal and X-ray diffraction techniques. Thermochim Acta 269-270:779–795. https://doi.org/10.1016/0040-6031(95)02571-5

Moropoulou A, Cakmak A, Labropoulos KC, Van Grieken R, Torfs K (2004) Accelerated microstructural evolution of a calcium-silicate-hydrate (C-S-H) phase in pozzolanic pastes using fine siliceous sources: comparison with historic pozzolanic mortars. Cem Concr Res 34:1–6. https://doi.org/10.1016/S0008-8846(03)00187-X

Moropoulou A, Bakolas A, Anagnostopoulou S (2005) Composite materials in ancient structures. Cem Concr Compos 27:295–300. https://doi.org/10.1016/j.cemconcomp.2004.02.018

Oliver RP, Cennini A, Val d'Elsa C, Thompson DV (2006) Il Libro dell'Arte. Italica. 11:114. https://doi.org/10.2307/476627

PAI (2006) Piano di assetto idrogeologico regione Sardegna. http://www.sardegnageoportale.it

Palmström A (1995) RMi – a rock mass characterization system for rock engineering purposes. Sci. York

Piovesan R, Siddall R, Mazzoli C, Nodari L (2011) The Temple of Venus (Pompeii): a study of the pigments and painting techniques. J

Archaeol Sci 38:2633–2643. https://doi.org/10.1016/j.jas.2011.05.021

Piovesan R, Dalconi MC, Maritan L, Mazzoli C (2013) X-ray powder diffraction clustering and quantitative phase analysis on historic mortars. Eur J Mineral 25:165–175. https://doi.org/10.1127/0935-1221/2013/0025-2263

Pollione MV (n.d.15 BC) De Architecture. Vol. II. In: Cesariano C, De Architectura Libri Dece, 1521, Como

Quattrocchi L (2018) The tomb mosaic of Fl(avius) Rogatianus at Forum Traiani (Oristano, Sardinia). SAGVNTVM Papeles del Lab Arqueol Val 49:161. https://doi.org/10.7203/sagvntvm.49.9980

Ramacciotti M, Rubio S, Gallello G, Lezzerini M, Raneri S, Hernandez E, Calvo M, Columbu S, Morales A, Pastor A, De la Guardia M (2019) Chemical and mineralogical analyses on stones from Sagunto Castle (Spain). J Archaeol Sci Rep 24:931–938. https://doi.org/10.1016/j.jasrep.2019.03.017

Raneri S, Pagnotta S, Lezzerini M, Legnaioli S, Palleschi V, Columbu S, Neri NF, Mazzoleni P (2018) Examining the reactivity of volcanic ash in ancient mortars by using a micro-chemical approach. Mediter Archaeol Archaeom. https://doi.org/10.5281/zenodo.1285897

Sağin EU, Böke H, Aras N, Yalçin Ş (2012) Determination of $CaCO_3$ and SiO_2 content in the binders of historic lime mortars. Mater Struct Constr 45:841–849. https://doi.org/10.1617/s11527-011-9802-1

Secco M, Dilaria S, Addis A, Bonetto J, Artioli G, Salvadori M (2018) The evolution of the Vitruvian recipes over 500 years of floor making techniques: the case studies of the Domus delle Bestie Ferite and the Domus di Tito Macro (Aquileia, Italy). Archaeometry. 60:185–206. https://doi.org/10.1111/arcm.12305

Secco M, Previato C, Addis A, Zago G, Kamsteeg A, Dilaria S, Canovaro C, Artioli G, Bonetto J (2019) Mineralogical clustering of the structural mortars from the Sarno Baths, Pompeii: a tool to interpret construction techniques and relative chronologies. J Cult Herit 40: 265–273. https://doi.org/10.1016/j.culher.2019.04.016

Serra PB, Bacco P (1998) Forum Traiani: il contesto termale e l'indagine archeologica di scavo. L'Africa Romana 7:1213–1255

Serra PB, Bacco P (2014) Aquae Ypsitanae – Forum Traiani: Mostra archeologico grafica, fotografica. Soprintendenza per i beni archeologici delle provincie di Cagliari ed Oristano

Siedel H (2018) Salt efflorescence as indicator for sources of damaging salts on historic buildings and monuments: a statistical approach. Environ Earth Sci 77. https://doi.org/10.1007/s12665-018-7752-4

Sitzia F (2019) Decay monitoring and conservation of Sardinia monumental heritage through geochemical, petro-physical and micro-photogrammetric characterization of stone surfaces. PhD thesis in Earth and Environmental Sciences and Technologies. University of Cagliari

Verdiani G, Columbu S (2010) E. Stone, an archive for the Sardinia monumental witnesses. Lecture notes in computer science. https://doi.org/10.1007/978-3-642-16873-4_27

Vola G, Gotti E, Brandon C, Oleson JP, Hohlfelder RL (2011) Chemical, mineralogical and petrographic characterization of Roman ancient hydraulic concretes cores from Santa Liberata, Italy, and Caesarea Palestinae. Israel Period di Mineral. https://doi.org/10.2451/2011PM0023

Wentworth CK (1922) A scale of grade and class terms for clastic sediments. J Geol 30:377–392. https://doi.org/10.1086/622910

Wetmore MN, Vitruvius Morgan MH (2010) Vitruvius: the ten books on architecture. Class Wkly 9:116. https://doi.org/10.2307/4387224

Zucca R (1986) Fordongianus, Sassari

Zucca R (2004) Viaggio nell'archeologia della provincia di Oristano. E.P.T, Oristano, Oristano